Nanometer size hole fabrication in 2d ultrathin films with cluster ion beams

Z. Insepov[1-3*], A. Ainabayev[1], S. Kirkpatrick[4], M. Walsh, Jr.[4], A.F. Vyatkin[5]

[1] Nazarbayev University, NURIS, 53 Kabanbay Batyr Ave., Astana, 010000, Kazakhstan
[2] Purdue University, School of Nuclear Engineering, 500 Central Drive, West Lafayette, IN, 47907 USA
[3] National Research Nuclear University MEPhI, Condensed Matter Physics Department, 31 Kashira Highway, 115409, Russian Federation
[4] Exogenesis Corp., 20 Fortune Drive, Billerica MA 01821, USA
[5] Institute of Microelectronics Technology and High Purity Materials, 6, Academician Ossipyan St., Moscow region, 142432, Russian Federation

ABSTRACT

Gas cluster ion beams are proposed as a new tool for producing nanometer sized holes in ultrathin 2D films. Surfaces of films of graphene, graphene oxide, MoS_2, and HOPG, and also silicon as a reference, were irradiated by Ar gas cluster ion beams (Exogenesis Corporation, Billerica, MA USA). The results were analyzed using atomic force microscopy (AFM) and Raman spectroscopy. Ar gas cluster ion acceleration energy was 30 keV and total ion fluences ranged from 1×10^{8} to 1×10^{13} cm^{-2}. Uniformly distributed holes, typically in the range of 10 to 25 nanometers in diameter, produced by the cluster ions, were observed on the surface of graphene oxide. To the best of our knowledge, this is first experimental observation of such holes

INTRODUCTION

Since the discovery by Novoselov and Geim in 2004 [1,2], ultrathin 2D films have witnessed an enormous increase of interest as prospective materials for various applications in condensed matter physics and chemistry. Graphene has attracted extensive interest due to its unique electronic, mechanical, optical and thermal properties [1-7]. These features of graphene are employed in different types of nanodevices such as transistors, sensors, and membranes [8-11]. Some of these graphene properties can be utilized for fabrication of ultrathin filters for water desalination and for purification of biological liquids, by introducing vacancies, holes, and defects or disorders in the graphene by means of energetic ion or laser beams. Lehtinen et al [12]

* Corresponding author Z. Insepov: zinsepov@purdue.edu

analyzed interactions with graphene of He, Ne, Ar, Kr, Xe, and Ga ions at various energies and incident angles using molecular dynamic (MD) and Monte Carlo (MC) methods to reveal changes in graphene structure during irradiation at macroscopic time scales. The results of their study can be useful to select processes for cutting and patterning of graphene by focused ion beams.

Nair et al [13] irradiated graphene with high-energy protons and carbon (C4+) ions to study influence of point defects induced by irradiation on magnetic properties of graphene. They concluded that point defects induced by irradiation lead to paramagnetism of graphene even for large defect densities and low temperature of 2 degrees. K. Pan et al [14] made in situ visualisation of defect introduction and amorphization in a single graphene layer under irradiation by 30 keV He or 6 keV Ar ions which can be useful to tune electronic and magnetic properties of graphene and for graphene processing by focused ion beams. Another topic of interest in ion irradiation of graphene is the possibility of membrane creation [15-18]. One of the ways to fabricate nanopores in a graphene sheet is to use electron beam irradiation [18]. However, low efficiency and high cost of the technique make it disadvantageous for wider application. Simulations and experiments show that nanopores with desired sizes can be formed by choosing appropriate ion irradiation parameters [19-21].

Another approach is that of using gas cluster ions beams (GCIB). Gas cluster ions are aggregates of a few hundreds to a few thousands of neutral gas atoms carrying a few positive charges induced by electron bombardment and subsequently accelerated by a high voltage [22, 23]. During contacting with a surface of target, cluster ions interact with many surface atoms simultaneously and transfer high energy to a very small region, thus creating damaged areas and pores [24]. To date, no previous experimental studies have been carried out to examine the effects of GCIB processing on the graphene. Several simulation studies have predicted formation of holes within graphene as a result of energetic Ar cluster ion bombardment [25-27]. Experimental investigations including GCIB irradiation of carbon have been performed so far on graphite and diamond surfaces only [27, 28].

Our preliminary results on modification of graphene and graphene oxide surfaces by gas cluster ions and highly-charged ions have been published elsewhere [29]. In the present study, experimental results of irradiation of graphene and graphene oxide with Ar gas cluster ion beams

are presented for the first time to the best of our knowledge. The irradiated samples were characterized with Raman spectroscopy and atomic force microscopy (AFM).

EXPERIMENTAL

Compressed argon gas was adiabatically expanded through a small nozzle into vacuum to create a supersaturated gas beam containing large Ar gas clusters. Each cluster consisted of several hundred to several thousand atoms bonded together by Van der Waals forces. The expanding supersonic jet consisting of clusters and of monomer atom gas was subjected to low energy electron bombardment to cause the clusters to become electrically charged with a few positive electronic charges. The ionized clusters were then accelerated by high voltages of up to several tens of kilovolts. Though the total energy of the accelerated clusters was high, the acceleration energy was shared among a large number of cluster atoms such that the individual atoms within the clusters had relatively low kinetic energies. Bombardment of a surface by a gas cluster ion beam allows modification and control of surface chemical and physical properties such as nanoscale smoothness, hydrophilicity and amorphization (see e.g. [22, 23] and the references in it).

In the present study, gas cluster ion beams (GCIB) of Ar were used to produce defects on a variety of 2D-materials, such as graphene oxide and graphene, MoS_2, highly oriented pyrolytic graphite (HOPG), and also on silicon as a reference. Irradiation was performed by Ar cluster ions with acceleration energy $E \approx 30$ keV (Exogenesis Corp., Billerica, MA, USA) and total fluence of Ar cluster ions ranged from 1×10^{8} to 1×10^{13} ions/cm^2.

The technology of gas cluster ion beam irradiation is a unique low energy method for surface treatment of ultrathin 2D films. When accelerated clusters interact with the surface of the processed material, the cluster ion does not penetrate deeper than a few atomic layers ($\leq$10 nm). Upon impact on a surface, clusters instantly create extreme transient conditions of temperature and pressure for the surface atoms [24]. Thus, cluster ions are an ideal tool for large defect fabrication on graphene and other 2D films and, since they do not penetrate deeply into the substrates, defects in the substrate are not created. Therefore, characterization of defects in the cluster beam irradiated 2D-films becomes much easier than for traditional monomer ion beams.

High quality graphene a few layers thick was obtained by epitaxial growth of hydrocarbons on top of nickel (4-7) and silicon substrates using a chemical vapor deposition

(CVD) method (Graphene Supermarket). Graphene oxide samples were prepared by spin coating of a stable suspension of GO crystallites obtained by Hummers method on the surface of silicon dioxide. The MoS_2 bulk samples were purchased from Structure Probe Inc.

The Raman spectroscopy study of the irradiated samples was conducted by a 632 nm laser wavelengths and 100× objective, and atomic force microscopy (AFM) measurements were carried out in a tapping mode.

RESULTS AND DISCUSSIONS

The analysis of irradiated samples conducted using AFM and Raman spectroscopy clearly prove the presence of defects in the form of nanopores on graphene oxide, amorphization/bumps, vacancy-like defects in graphene and formation of holes on the surface of silicon, MoS_2 and HOPG.

Silicon and HOPG

Polished Si substrates with a native oxide and HOPG (Figure 1,2) were exposed to a 1×10^{10} cm^{-2} fluence of 30 keV acceleration energy Ar clusters. AFM images of irradiated silicon surfaces show formation of craters. Figure 1a shows a 0.5×0.5 μm AFM image of a silicon surface exhibiting craters with dimensions of about 20 nm in diameter and 1 nm deep. Figure 1b is a histogram of the crater diameter distribution on the sample. The distribution appears to be consistent with known Gaussian mass-to-charge size ratio distributions of individual clusters ranging from about 1000 atoms per cluster to roughly 10000 atoms per cluster, as determined by time-of-flight measurements [22].

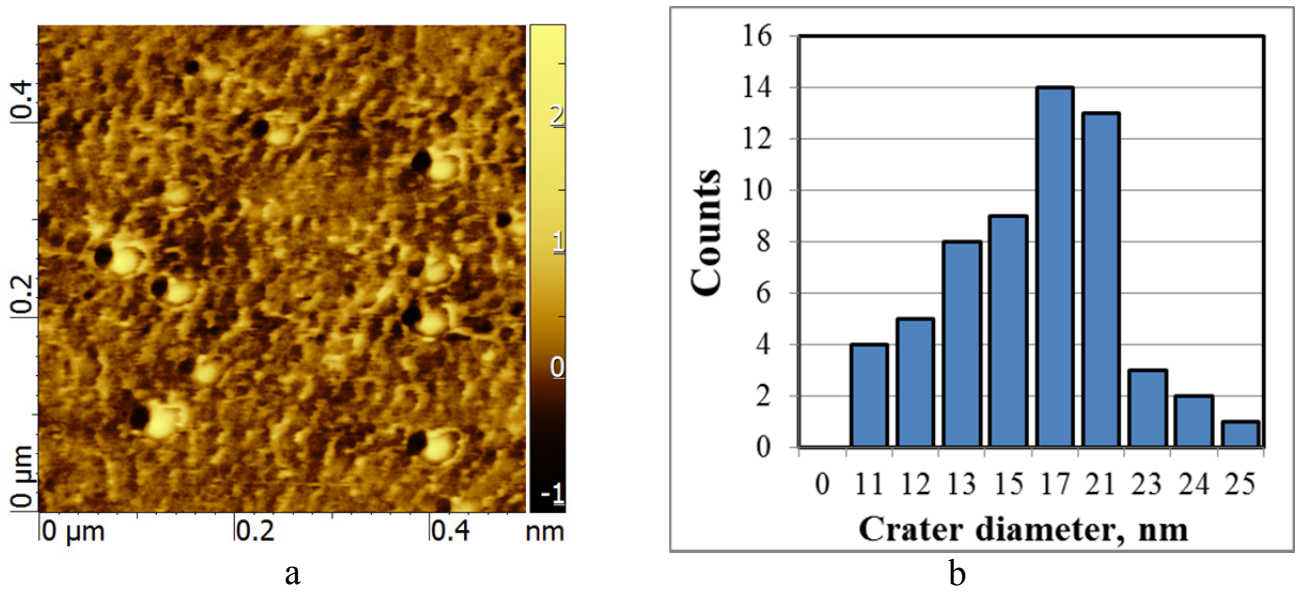

a b

Figure 1. AFM images of GCIB irradiated Si sample a) craters on surface for a 0.5×0.5 µm scan area; b) histogram of crater diameters distribution on silicon sample.

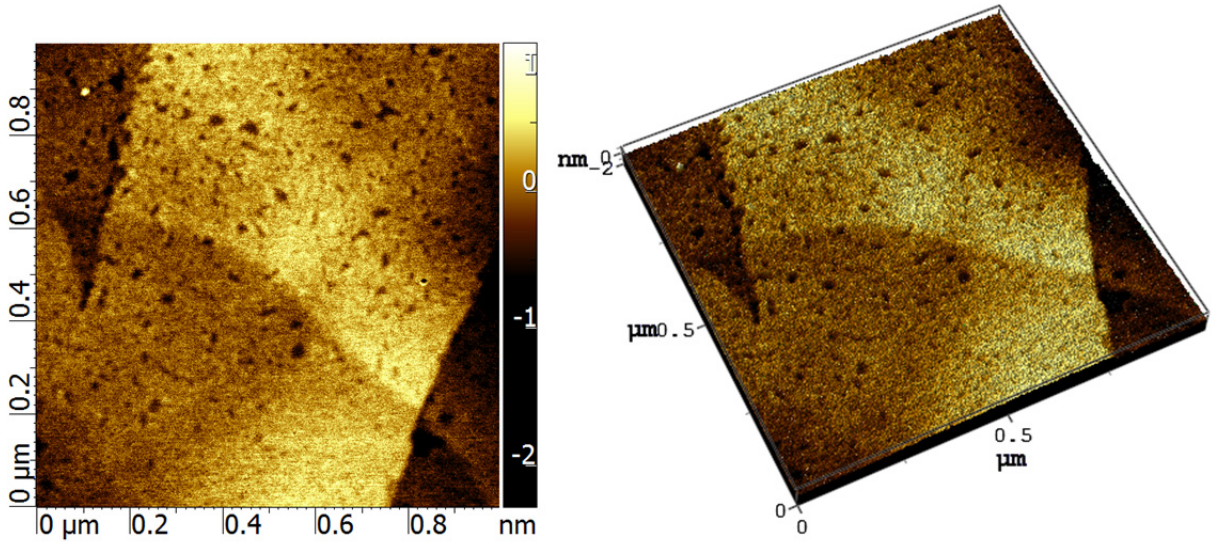

a b

Figure 2. AFM image of HOPG surface irradiated by clusters with ion dose 1×10^{10} clusters/cm^2 a) craters on surface for a 1×1 µm scan area; b) 3D view of the same surface.

Figure 2 shows 1×1 μm^2 AFM images of a HOPG surface exhibiting craters with average diameters of 10 nm and average depth of 1.5 nm. The holes were observed at a cluster ion beam dose of 10^{10} ions/cm^2.

Graphene oxide

Graphene oxide samples were irradiated at an angle less than 45 degrees, and the irradiation dose was varied from 1×10^9 to 1×10^{11} cm^{-2}. Small pores created on the graphene oxide surfaces were found to have a mean pore size of 11-13 nm and a depth of 2-4 nm. Example AFM images are shown in Figures 3a, 3c and 3d.

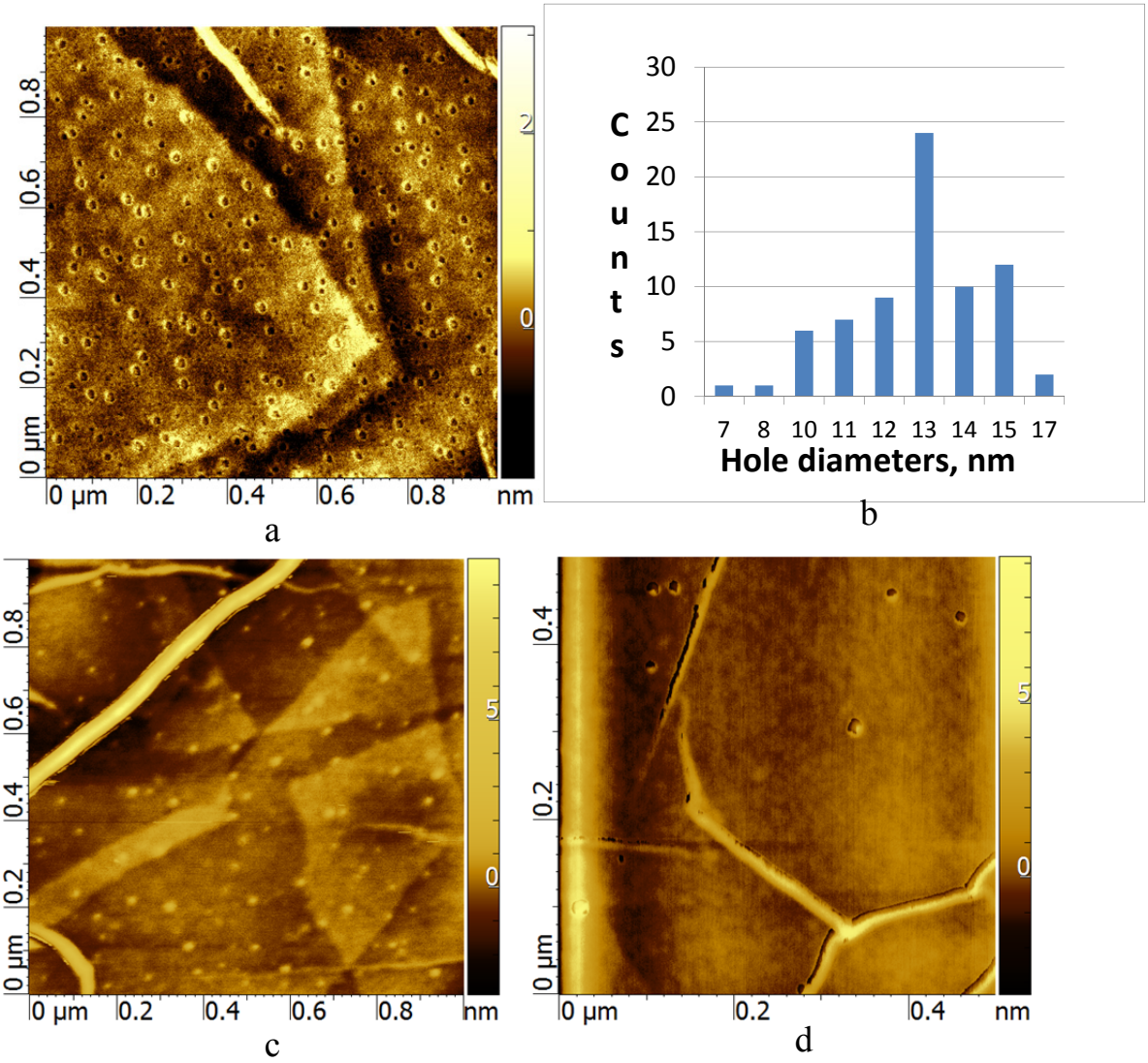

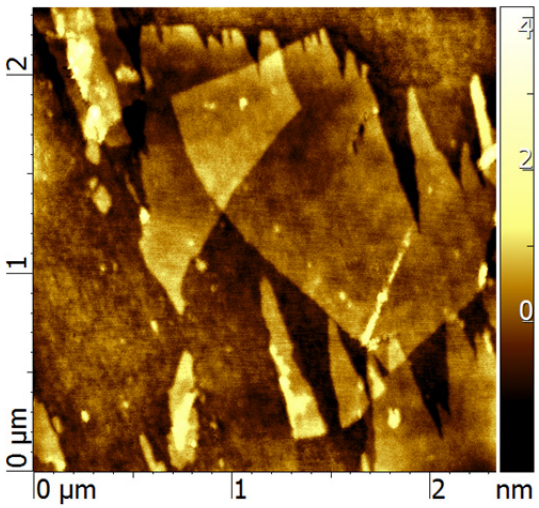

e

Figure 3. AFM images of graphene oxide sample with holes and bumps on surface 1×1 μm^2 irradiated with GCIB, with irradiation dose a) 1×10^{11} cm^{-2} b) histogram of hole diameter distribution on graphene oxide samples c) 1×10^{10} cm^{-2} d) 1×10^{9} cm^{-2} e) AFM image of graphene oxide before irradiation (Scan area 2.34 × 2.34 μm^2).

Figure 3b shows a histogram for hole diameters of GCIB induced defects on a graphene oxide surface. For reference, an image of a graphene oxide surface before irradiation is given in Figure 3e. Comparison of the images in Figures 3a, 3c, and 3d with the image in Figure 3e from similar graphene oxide surface before GCIB exposure reveals the effect of irradiation with gas clusters on graphene oxide structure.

Thus, AFM characterization distinctly displays formation of holes on graphene oxide surface and craters on silicon and HOPG samples.

Graphene

Graphene samples were irradiated at acceleration energy 30 keV with doses in the range of 1×10^{8} to 1×10^{13} ions/cm^2. Figure 4a shows an irradiated sample of a few layer graphene film on Ni with fluence 1×10^{13} ions/cm^2. It can be seen that there are some amorphization type defects distributed on the surface of the graphene. For comparison, Figure 4b shows a non-

irradiated region of the same graphene sample, where it can be seen that surface roughness Rms = 2.61771 nm was significantly lower than after cluster ion beam irradiation as displayed on Figure 5a where Rms is equal to 3.78283 nm.

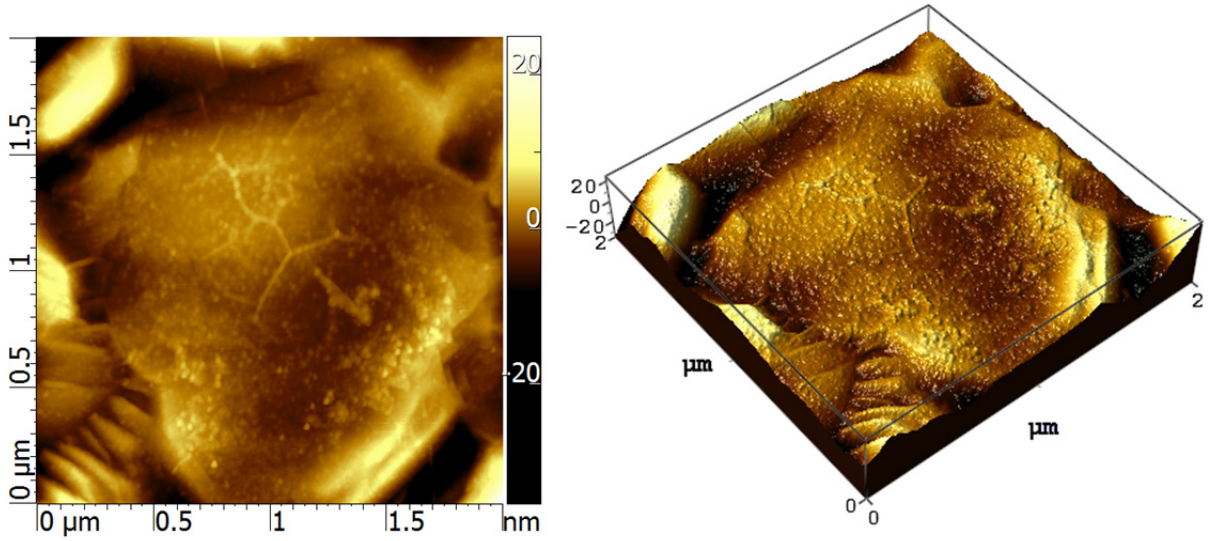

a

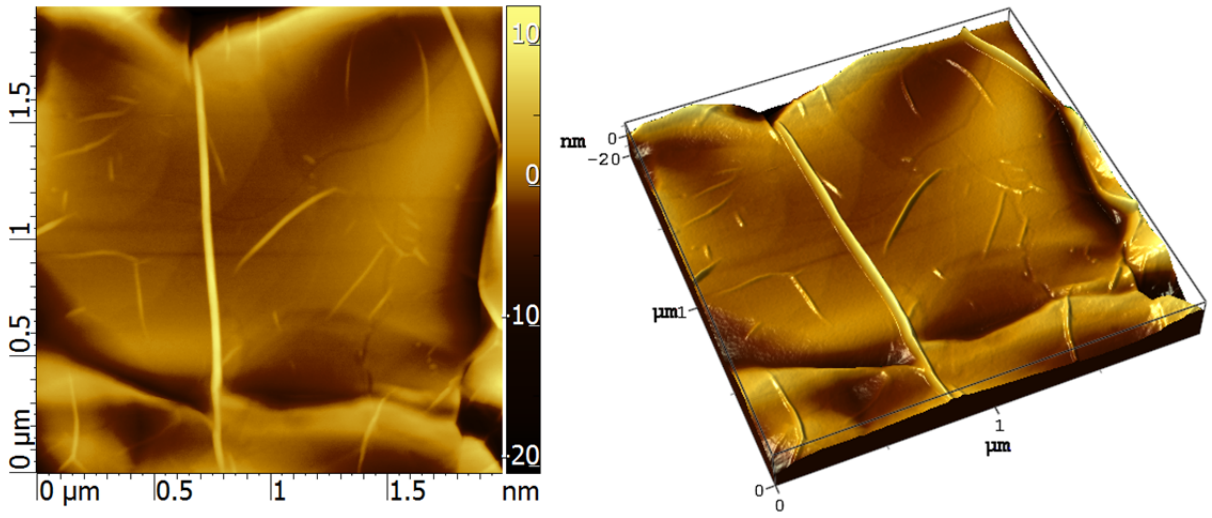

b

Figure 4. The samples of graphene on Ni 2×2μm^2; a) Graphene film irradiated with a dose of 1×10^{13} ions/cm^2 and b) non-irradiated area of the sample.

In general, AFM characterizations made in tapping mode show that ion cluster fluence 1×10^{13} cm^{-2} seems to be a threshold for formation of defects on graphene. At lower fluences ranging from 1×10^9 to 1×10^{12} cm^{-2} no defects were observed by AFM. Moreover, in the case of single/double layer graphene, even irradiation with fluence of 1×10^{13} cm^{-2} would most likely not be sufficient to create defects that can be observed by AFM in tapping mode.

Molybdenum disulphide

Bulk samples of MoS_2 were irradiated by Ar gas cluster ions with energy 30 keV and doses ranging from 10^9 to 10^{11} ions per cm^2. In the case of MoS_2 samples we were able to find holes only for samples where the irradiation dose was 10^{10} ions per cm^2 . Craters that were observed, shown in Figure 5a, had diameters of approximately 13-16 nm and depths of 0.7-0.8 nm. For comparison purposes, the non-irradiated bulk MoS_2 surface AFM image is shown in figure 5b.

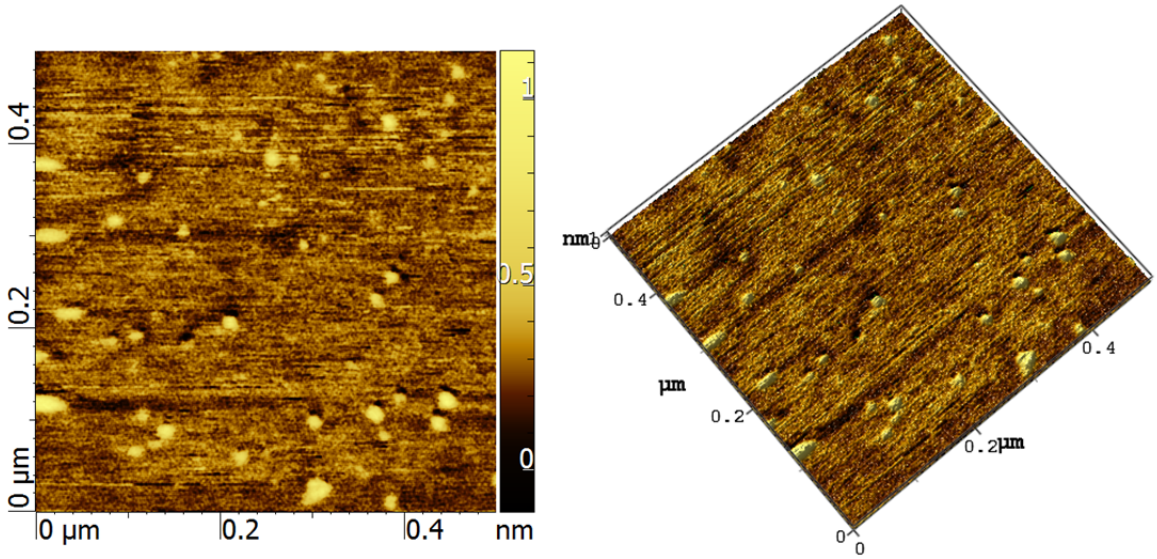

a

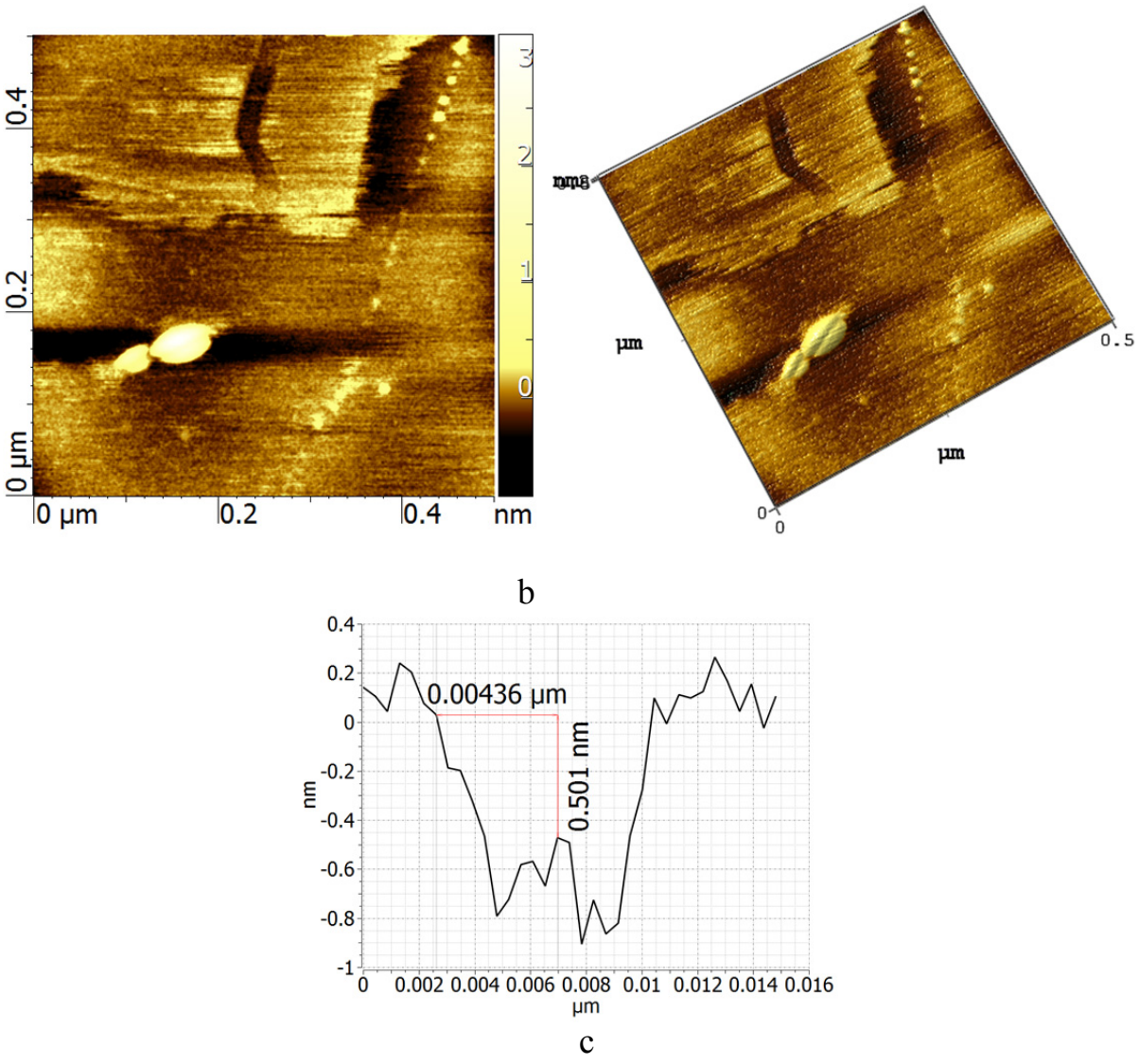

Figure 5. The samples of bulk molybdenum disulphide 0.5×0.5µm^2; a) irradiated with a dose of 1x10^{10} ions/cm^2 , b) non-irradiated area of the sample and c) cross section view of crater.

Raman spectra of GCIB irradiated samples of graphene

Raman spectroscopy is a universally recognized method for characterizing the irradiated graphene films [30]. Raman spectra of graphene are characterized by three main peaks. The first peak, the G peak (1582-1588 cm^{-1}), corresponds to a transition with the emission of an optical phonon E2g at the Γ point of the Brillouin zone, corresponding to the planar vibrations of the carbon atoms in the plane of the layers [31]. Its intensity depends on the number of layers. The

more layers, the more intense the G-peak. The presence of a narrow G-peak (less than 50 cm-1) indicates an ordered local hexagonal structure of carbon atoms. The second peak is the D peak (1340 - 1360 cm^{-1}). Its origin is due to resonant Raman scattering by an optical phonon near the K or K′ point of the Brillouin zone and related breathing modes of the hexagonal sp2 carbon rings. In pure and in perfect samples of graphene this peak is absent; however, it appears in the presence of an additional scattering channel on the defects. In this regard, the D-peak is often called "defective" [31]. More specific information on the local number of graphene monolayers can be obtained from the analysis of the 2D peak (2600 - 2700 cm-1), which is the overtone of the D peak. The shape, width, and position of the 2D peak depend on the number of layers of graphene. In monolayer graphene, the 2D peak is a singlet. It is considered that if the intensity of the 2D peak exceeds the intensity of the peak G by 2 or more times, then the graphene consists of one layer [31].

Our Raman spectroscopy study of irradiated graphene samples shows some defects in single/double layer graphene irradiated with 1×10^{12} to 1×10^{13} ions/cm^2 while fluences lower than 1×10^{11} ions/cm^2 are not sufficient to create defects in graphene (Figure 6).

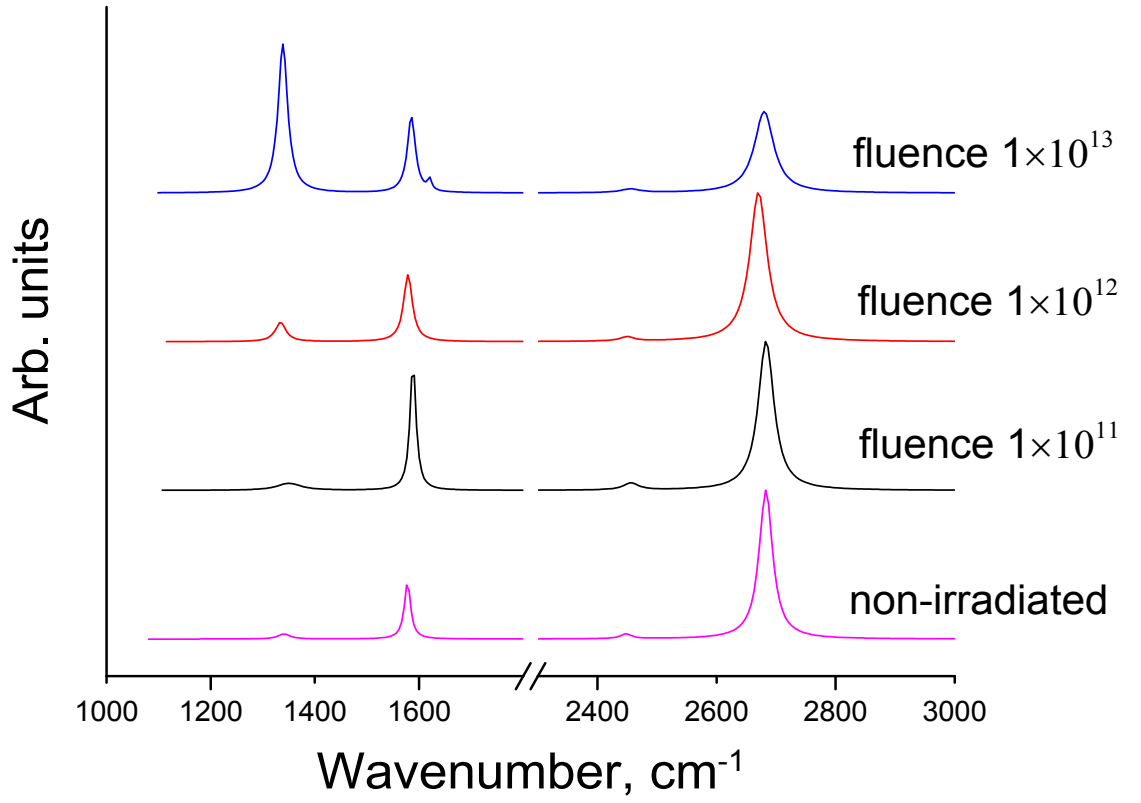

Figure 6. Raman spectra of single/double layer graphene irradiated with 1×10^{11}-1×10^{13} ions/cm^2 fluence.

Figure 6 shows Raman spectra of single/double layer graphene irradiated with 1×10^{11} to 1×10^{13} ions/cm^2 fluence and also pristine single/double layer graphene for reference. It can be seen that with increase of ion fluence the amount of damage increases which can be seen from increase of intensity ratio of D peak to G peak, since it is well established that D peak corresponds to amount of damage in graphene structure. Similar results were obtained in work [32] where it was found that level of damage that was caused by cluster ion beam is a function of ion beam dose and kinetic energy per atom (E/n) in the cluster ions. In this work [32] irradiation of single layer graphene with cluster consisted of 2000 atoms of Ar with energy 10 keV and ion dose 1 ions/nm^2 (converting to cm^2 gives 1×10^{14} ions/cm^2) gives the similar pattern of Raman spectra of irradiated graphene as in our case for fluence 1×10^{13} ions/cm^2 and energy 30 keV.

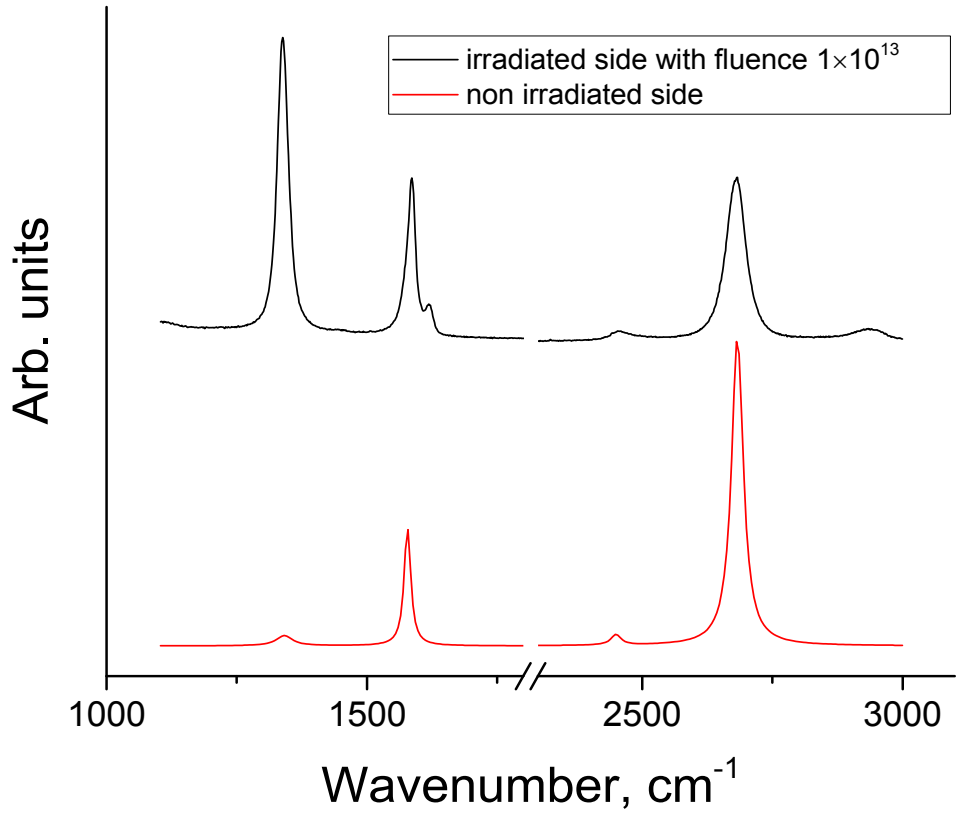

Figure 7. 633 nm Raman spectrum of single/double layer graphene on a 285 nm SiO_2 film irradiated with cluster ion beam, with fluence 1×10^{13} cm^{-2}.

The prominent changes in Raman spectra can be seen for single/double layer graphene on (285 nm) SiO_2 irradiated with cluster ion beam, with fluence 1×10^{13} cm^{-2} (Figure 7). Figure 7 shows that apart from the main three Raman peaks of graphene after gas cluster irradiation there is one more peak - D′-peak (at ~1620 cm^{-1}) which comes from optical phonons at K or K′ points in the first Brillouin zone attributed to an intravalley double resonance process [31]. The ratio of intensities of D and D′ peaks indicates type of defects present in graphene structure. It was shown [33] that when ratio of $I_D/I_{D'}$ approximately equal to:

- ≈ 13-> sp3 defects,
- ≈ 7-> sp2 or "vacancy-like" defects,
- ≈ 4-> boundary defects

are existing in structure of graphene. Relying on the results from ref. [33] we can conclude that appearance of D′ and ratio of $I_D/I_{D'} \approx 7$ on Raman spectra in Figure 8 indicates that there should be vacancy like defects and giving that $I_D/I_G \approx 1/L_D^2$ the distance between defects [34], L_D is equal to 2.5 nm. Raman spectroscopy of this sample shows that there is a high degree of disorder in graphene structure upon irradiation with high fluence more than 1×10^{12} cm^{-2} and energy 30 keV.

Raman spectroscopy was also performed on irradiated samples of molybdenum disulphide. Raman spectroscopy can be used to obtain an idea of the vibrational properties of MoS_2, as well as changes in the crystal lattice induced by doping [35] or deformation [36]. The Raman spectrum of bulk MoS_2 is characterized by two notable peaks, designated as E12g (~ 382 cm-1) and A1g (~ 407 cm-1); The first-order modes are related to the inside-plane and out-plane oscillations, respectively. When the thickness of MoS_2 decreases, the frequency of E12g begins to shift to an increased frequency, while the frequency A1g decreases until the frequency difference between the two peaks reaches ~ 19 cm-1 characteristic of single-layer MoS2, which makes it possible to identify the number of MoS2 layers [37].

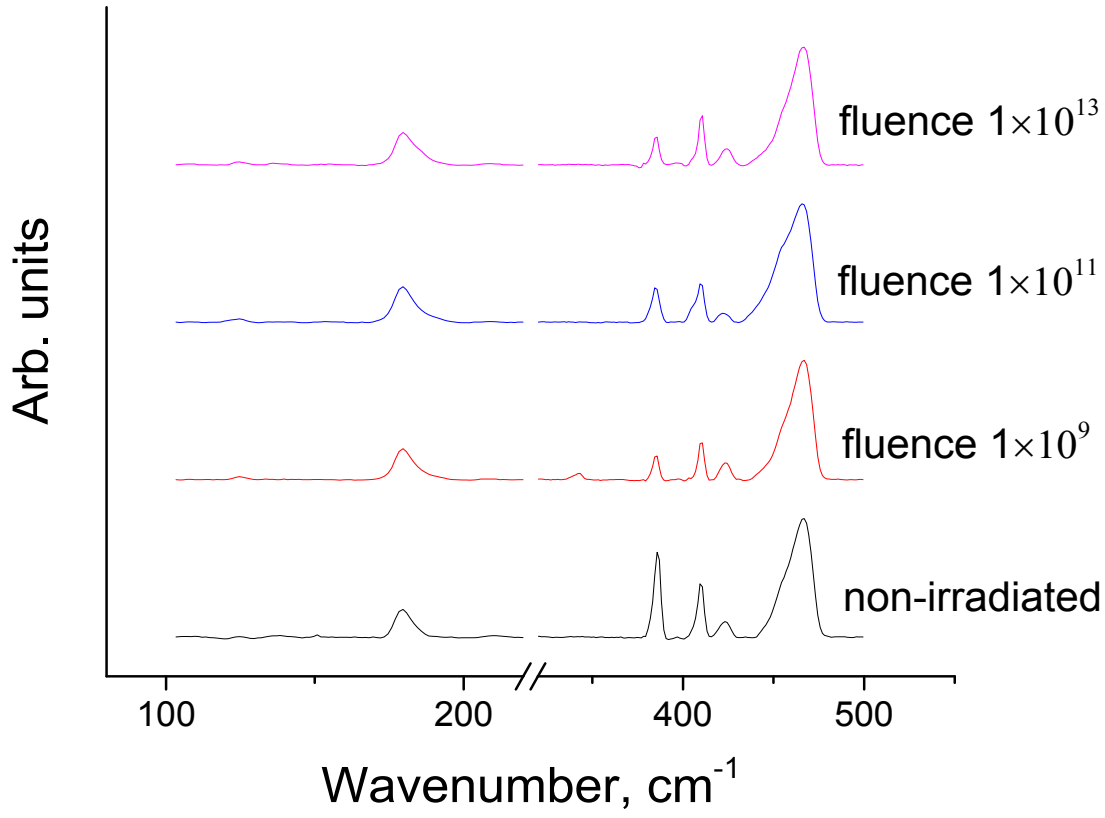

Figure 8. Raman spectra of irradiated samples of molybdenum disulphide

Figure 8 shows the Raman spectra of bulk samples of molybdenum disulphide irradiated with cluster ions at different ion beam doses. To date, very little work has been done to study the effect of particle irradiation on the molybdenum disulphide Raman spectrum, and on the whole such work was observed on thin molybdenum disulphide films (the Raman spectrum of thin films and bulk samples of molybdenum disulfide differ significantly), so unambiguous conclusions on Raman spectroscopy of molybdenum disulphide samples irradiated by cluster ions are difficult to make at this moment [33]. Nevertheless, according to the Raman spectra in the figure, our experiments showed an increase in the irradiation dose leading to a decrease in the intensity of the Raman disulfide peak of the molybdenum disulfide spectrum at the values 384.48 and 408.22.

CONCLUSIONS

Gas cluster ions were used for experimental confirmation of producing holes and craters on silicon, HOPG, graphene oxide (GO), and MoS_2 surfaces. Atomic force microscopy (AFM) and Raman spectroscopy characterization show that GCIB irradiation can create vacancy-like defects in single/double layer graphene, and small bumps on few layer graphene. We could not confirm production of holes on graphene with gas cluster ions for the total cluster energies of 30 keV, with the energy per atom of 10-20 eV/atom.

Instead, gas cluster ions at a high dose of 1×10^{13} ions/cm^2 create small bumps on a few layer graphene that are seen on the AFM images.

To understand better the details of interaction of cluster ions with 2D-materials and to optimize the irradiation process for hole fabrication, density functional and atomistic simulations were performed for the same 2D-materials, and the obtained results will be published elsewhere.

Acknowledgements

This work has been supported by the Ministry of Education and Sciences of Kazakhstan (Contract No. 265 -12.02.2015). Z.I. is indebted to the Nazarbayev University World Science Stars grant No. 031-2013 of 12/3/2013 and No.147, 3.03.2017. This work was in part funded by the Ministry of Education and Science of Russia, grant No.14.607.21.0047 (RFMEFI60714X0047).

REFERENCES:

1. K. S. Novoselov, A. K. Geim, S. V. Morozov, D. Jiang, Y. Zhang, S. V. Dubonos, I. V. Grigorieva, and A. A. Firsov, *Science* 306, 666 (2004).
2. K. S. Novoselov, E. McCann, S. V. Morozov, V. I. Fal'ko, M. I. Katsnelson, U. Zeitler, D. Jiang, F. Schedin, and A. K. Geim, *Nat. Phys.* 2, 177 (2006).
3. Y. Zhu, S. Murali, W. Cai, X. Li, J. W. Suk, J. R. Potts, and R. S. Ruoff, *Adv. Mater.* 22, 3906 (2010).
4. C. Lee, X. Wei, J. W. Kysar, and J. Hone, *Science* 321, 385 (2008). 11.
5. K. F. Mak, M. Y. Sfeir, Y. Wu, C. H. Lui, J. A. Misewich, and T. F. Heinz, *Phys. Rev. Lett.* 101, 196405 (2008).

6. Y. M. Zuev, W. Chang, and P. Kim, *Phys. Rev. Lett.* 102, 096807 (2009).
7. Z. M. Liao, B. H. Han, Y. B. Zhou, and D. P. Yu, *J. Chem. Phys.* 133, 044703 (2010).
8. K. S. Novoselov, V. I. Fal′ko, L. Colombo, P. R. Gellert, M. G. Schwab & K. Kim, *Nature* 490, 192 (2012).
9. S. Hu, M. Lozada-Hidalgo, F. C. Wang, A. Mishchenko, F. Schedin, R. R. Nair, E. W. Hill, D. W. Boukhvalov, M. I. Katsnelson, R. A. W. Dryfe, I. V. Grigorieva, H. A. Wu and A. K. Geim *Nature* 516, 227 (2014) .
10. Y-B. Zhou, Z-M. Liao, Y-F. Wang, G. S. Duesberg, J. Xu, Q. Fu, X.-S. Wu and D.-P. Yu, *J. Chem. Phys.* 133, 234703 (2010).
11. H. Zhang, Ultrathin Two-Dimensional Nanomaterials, ACS Nano, 9, 9451-9469 (2015).
12. O. Lehtinen, J. Kotakoski, A.V. Krasheninnikov & J. Keinonen, *Nanotechnology* 22, 175306 (2011).
13. R. R. Nair, M. Sepioni, I-Ling Tsai, O. Lehtinen, J. Keinonen, A. V. Krasheninnikov, T. Thomson, A. K. Geim and I. V. Grigorieva, Nature Phys 8, 199–202 (2012).
14. C.-T. Pan, J. A. Hinks, Q. M. Ramasse, G. Greaves, U. Bangert, S. E. Donnelly and S. J. Haigh, *Scientific reports* | 4 : 6334 | doi: 10.1038/srep06334
15. S. C. O'Hern, M. S. H. Boutilier, J-C. Idrobo, Y. Song, J. Kong, T. Laoui, M. Atieh, and R. Karnik, *Nano Lett.,* 2014, 14 (3), pp. 1234–1241.
16. O. Lehtinen, J. Kotakoski, A. V. Krasheninnikov, A. Tolvanen, K. Nordlund, and J. Keinonen, *Phys. Rev. B* 81, 153401 (2010).
17. E. H. Ahlgren, J. Kotakoski, O. Lehtinen, and A. V. Krasheninnikov, *Appl. Phys. Lett.* 100, 233108 (2012).
18. M.D. Fischbein, M. Drndić, *Appl. Phys. Lett.* **2008***, 93*, 113107.
19. R. Ritter, R. A.Wilhelm, M. Stöger-Pollach, R. Heller, A. Mücklich, U. Werner, H. Vieker, A. Beyer, S. Facsko, A. Gölzhäuser, *Appl. Phys. Lett.* **2013***, 102*, 063112.
20. W. Li, L. Liang, S. Zhao, S. Zhang, J. Xue, *J. Appl. Phys.* **2013***, 114*, 234304.
21. S. Standop, O. Lehtinen, C. Herbig, G. Lewes-Malandrakis, F. Craes, J. Kotakoski, T. Michely, A. V. Krasheninnikov, C. Busse, *Nano Lett.* **2013***, 13*, 1948-1955.
22. I. Yamada, J. Matsuo, N. Toyoda, A. Kirkpatrick, *Materials Science and Engineering: R: Reports* **2001***, 34*, 231-295.

23. I. Yamada, Materials Processing by Cluster Ion Beams: History, Technology, and Applications, CRC Press, 2015.
24. Z. Insepov, *Cluster Ion-Solid Interactions: Theory, Simulation, and Experiment*, Chapman and Hall/CRC, 2016.
25. N. Inui, K. Mochiji, K. Moritani, N. Nakashima, *Applied Physics A* **2010***, 98*, 787-794.
26. S. Zhao, J. Xue, L. Liang, Y. Wang, S. Yan, *The Journal of Physical Chemistry C* **2012***, 116*, 11776-11782.
27. Y. Yamaguchi, J. Gspann, T. Inaba, *The European Physical Journal D-Atomic, Molecular, Optical and Plasma Physics* **2003***, 24*, 315-318.
28. V. Popok, J. Samela, K. Nordlund, V. P. Popov, *Nuclear Instruments and Methods in Physics Research Section B: Beam Interactions with Materials and Atoms* **2012***, 282*, 112-115.
29. Z. Insepov, A. Ainabayev, K. Dybyspayeva, A. Zhuldassov, S. Kirkpatrick, M. Walsh and A.F. Vyatkin, MRS Advances, Vol.1, Issue 20 (Nanomaterials and Synthesis) 2016, pp. 1417-1422.
30. L. G. Cancado,; A. Jorio, E. H. M. Ferreira, F. Stavale, C. A. Achete, R. B. Capaz, M. V. O. Moutinho, A. Lombardo, T. S. Kulmala, A. C. Ferrari, Nano Lett. 2011, 11 (8), 3190.
31. A. C. Ferrari, D. M. Basko, Nature Nanotechnology, 8 (2013)|
32. B. J. Tyler, B. Brennan, H. Stec, T. Patel, L. Hao, I. S. Gilmore, and A. J. Pollard , J. Phys. Chem. C 2015, 119, 17836−17841
33. A. Eckmann , A. Felten, A. Mishchenko, L. Britnell, R. Krupke, K. S. Novoselov, and C. Casiraghi, *Nano Lett.,* 2012, 12 (8), pp 3925–3930.
34. M. M. Lucchese, F. Stavale, E. H. Ferriera, C. Vilane, M. V. O. Moutinho, R. B. Capaz, C. A. Achete, A. Jorio, Carbon 2010, 48, 1592–1597.
35. B. Chakraborty, A.Bera, D. V. S.Muthu, S.Bhowmick, U. V. Waghmare, and A. K.Sood // Phys. Rev. B. – 2012. – V. 85, 161403(R).
36. C. Rice, R. J. Young, R. Zan, U. Bangert, D. Wolverson, T. Georgiou, R. Jalil, and K. S. Novoselov // Phys. Rev. B. – 2013. – V. 87, 081307(R).
37. C. Lee, H. Yan, L. E. Brus, T. F. Heinz, J. Hone, and S. Ryu // ACS Nano. – 2010. – V. 4. – P. 2695.

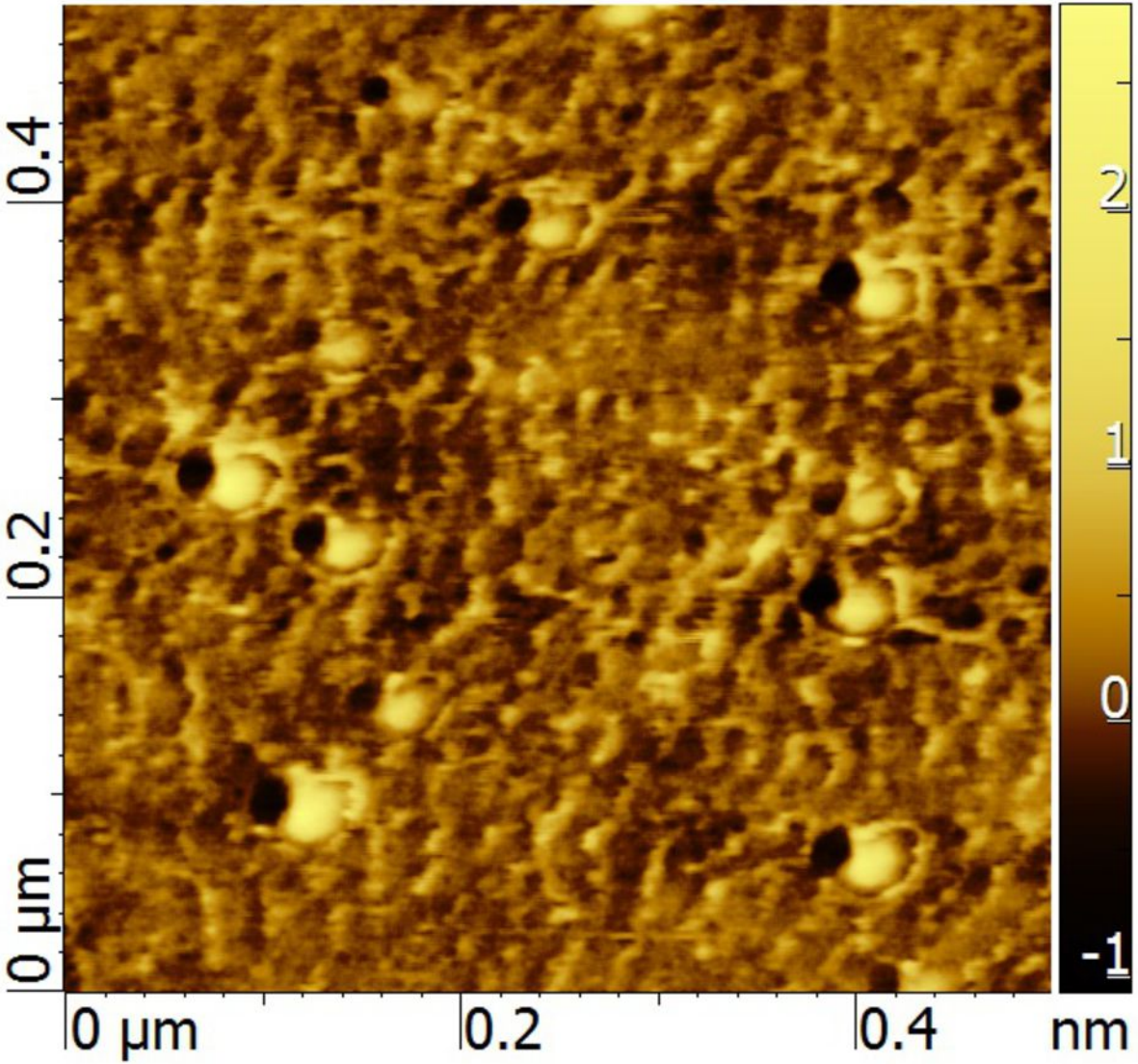
0.4
0.2
0 µm
0 µm
0.2
0.4
nm
2
1
0
-1

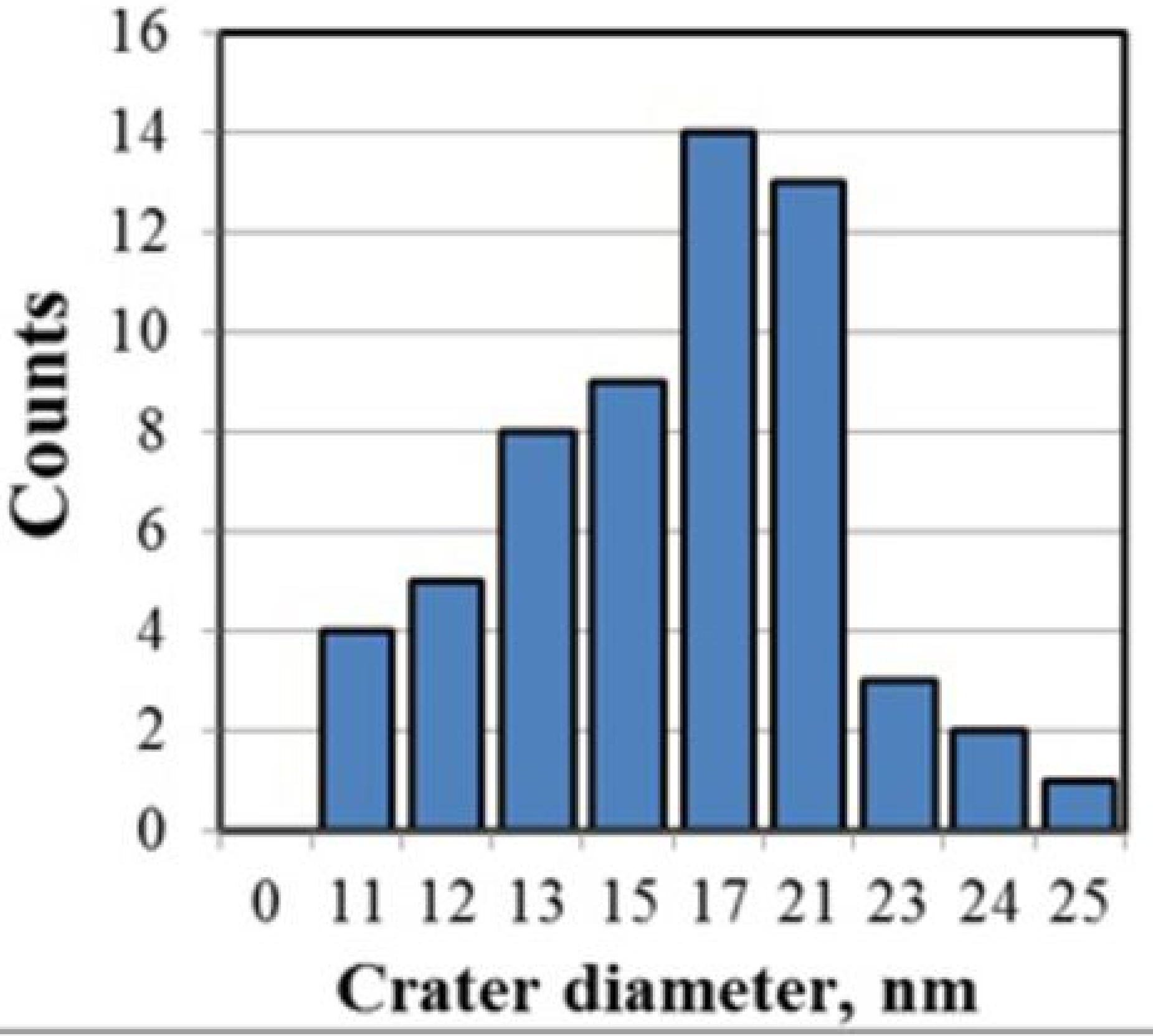
16
14
12
10
8
6
4
2
0
Counts
0
11
12
13
15
17
21
23
24
25
Crater diameter, nm

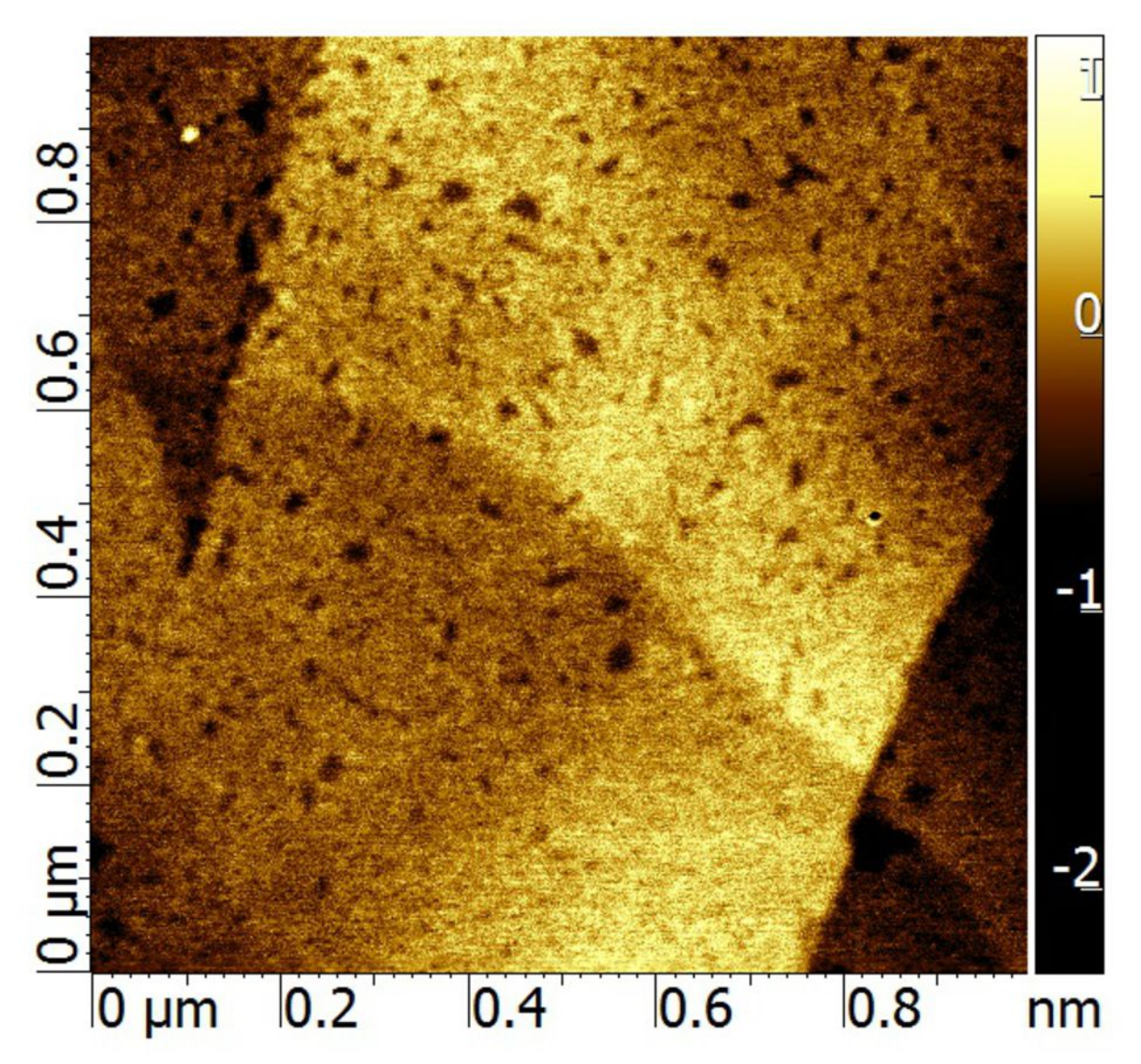
0 µm
0.2
0.4
0.6
0.8
nm
0 µm
0.2
0.4
0.6
0.8
0
-1
-2

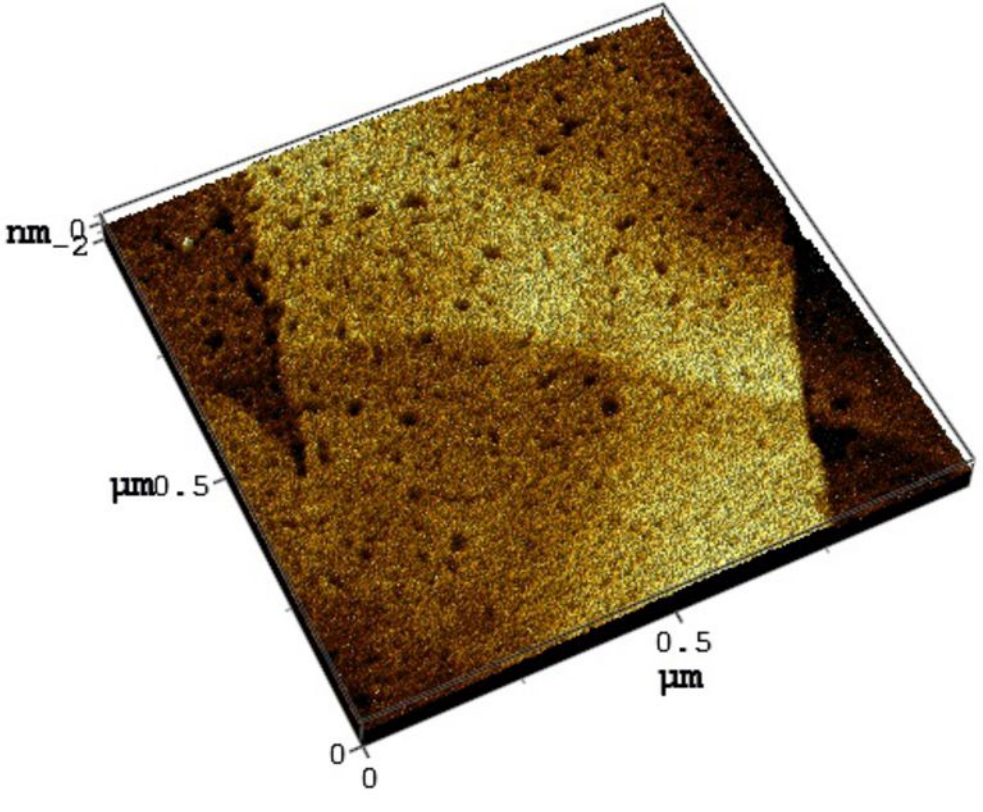
nm_0
2
µm0.5
0
0
0.5
µm

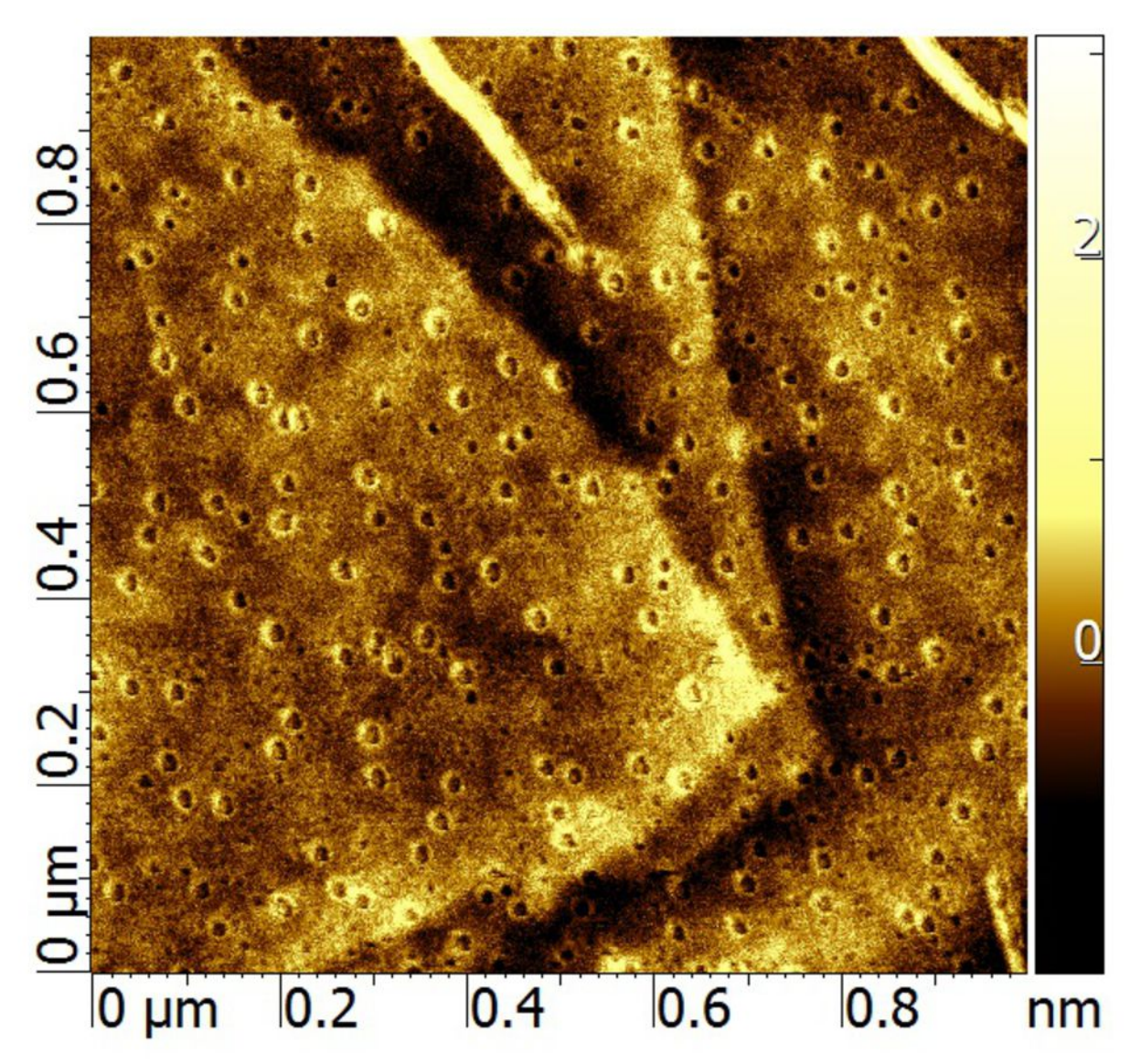
0.8
0.6
0.4
0.2
0 µm
2
0
0 µm
0.2
0.4
0.6
0.8
nm

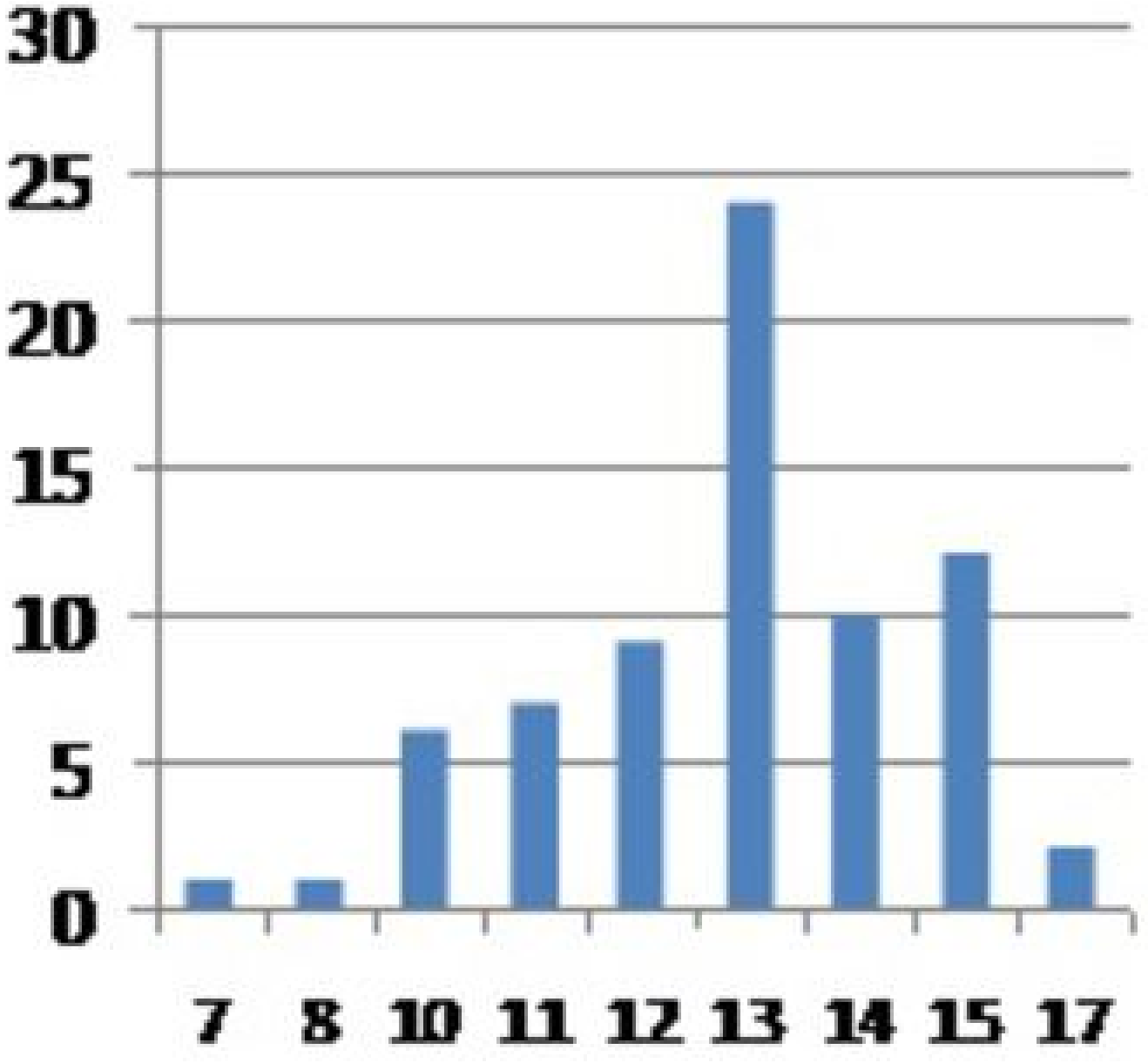
30
25
20
15
10
5
0
7
8
10
11
12
13
14
15
17

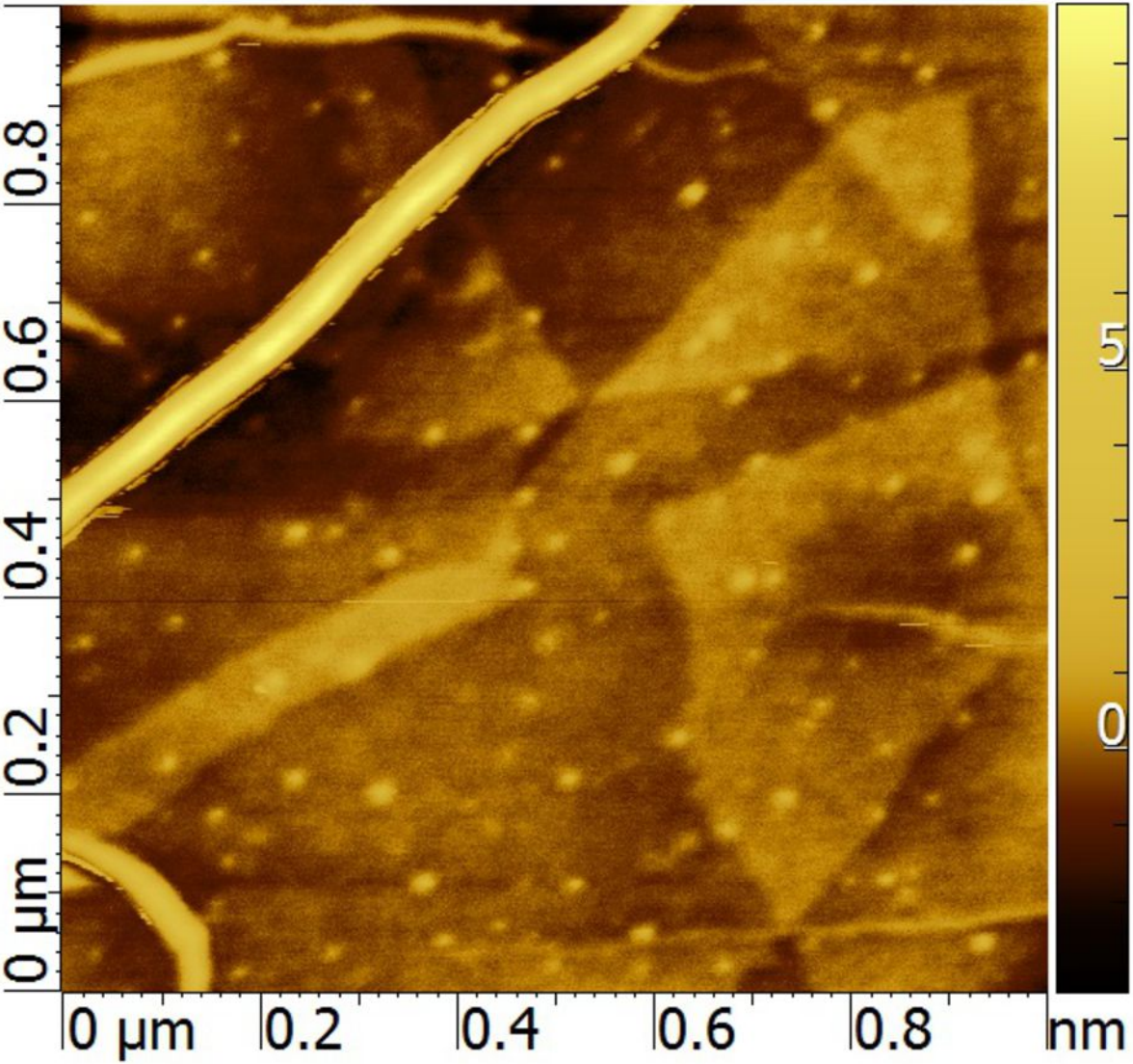
0.8
0.6
0.4
0.2
0 µm
5
0
0 µm
0.2
0.4
0.6
0.8
nm

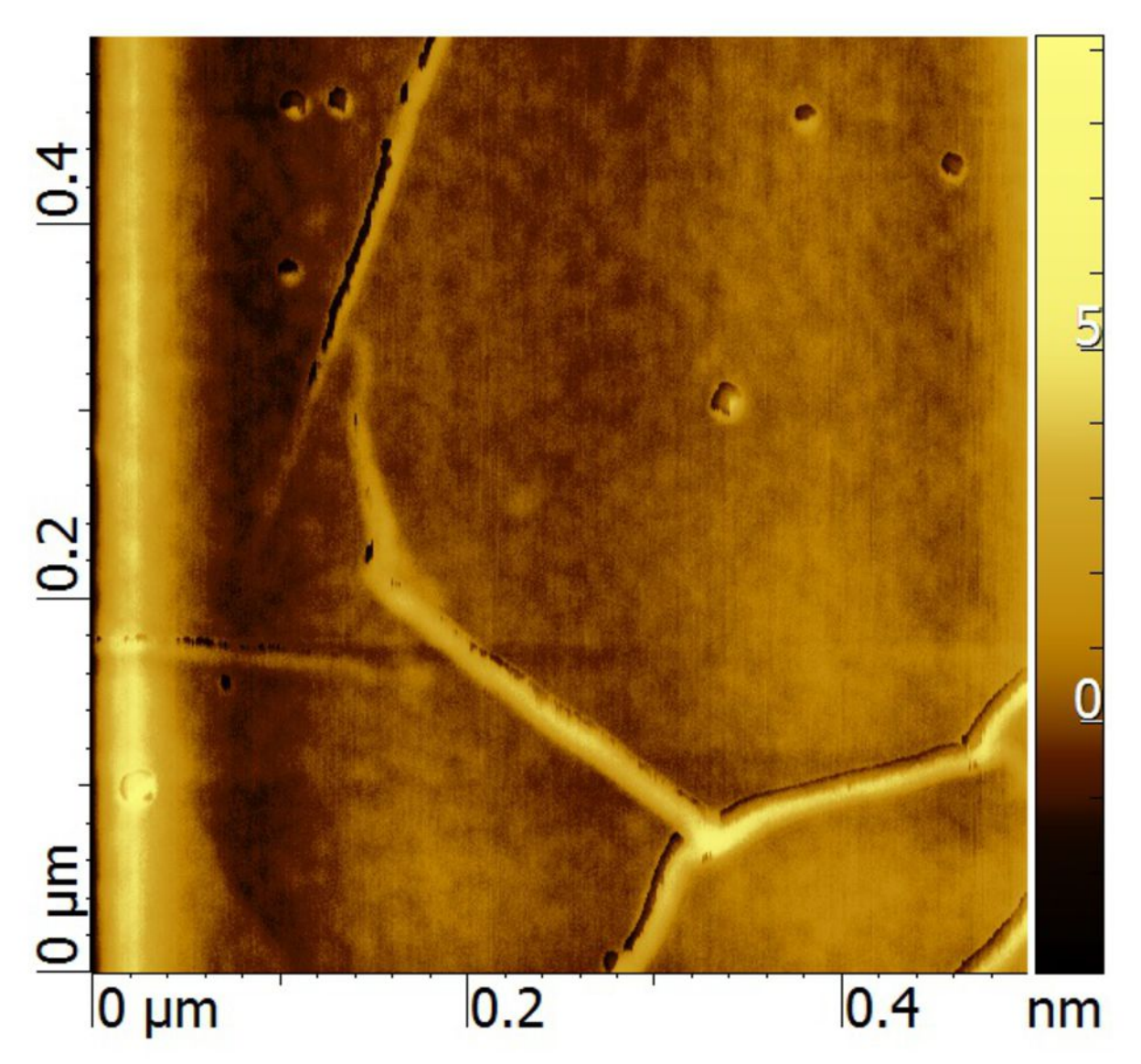
0.4
0.2
0 µm
0 µm
0.2
0.4
nm
5
0

2
1
0 µm
0 µm
1
2
nm
4
2
0

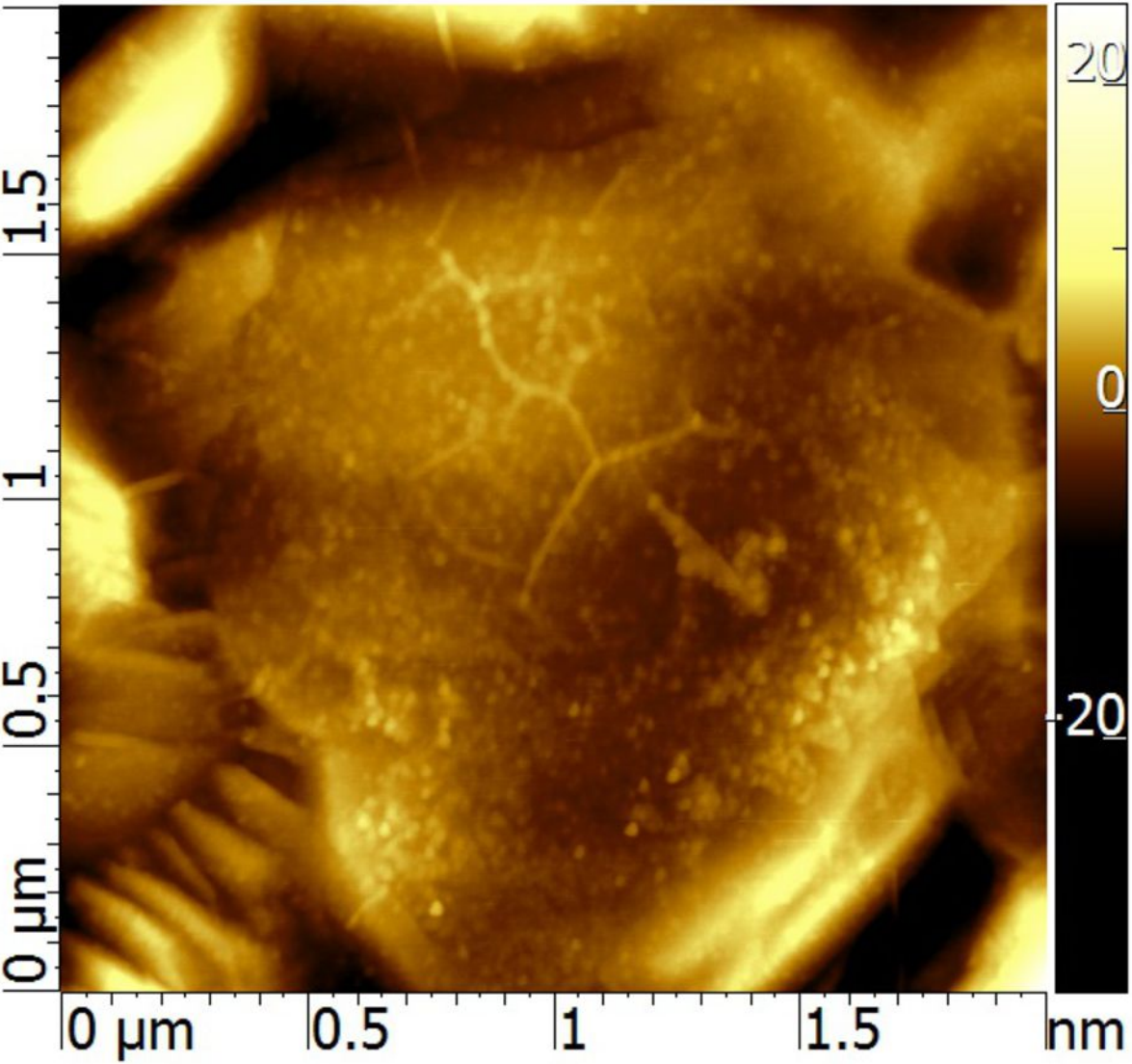
20
0
-20
1.5
1
0.5
0 µm
0 µm
0.5
1
1.5
nm

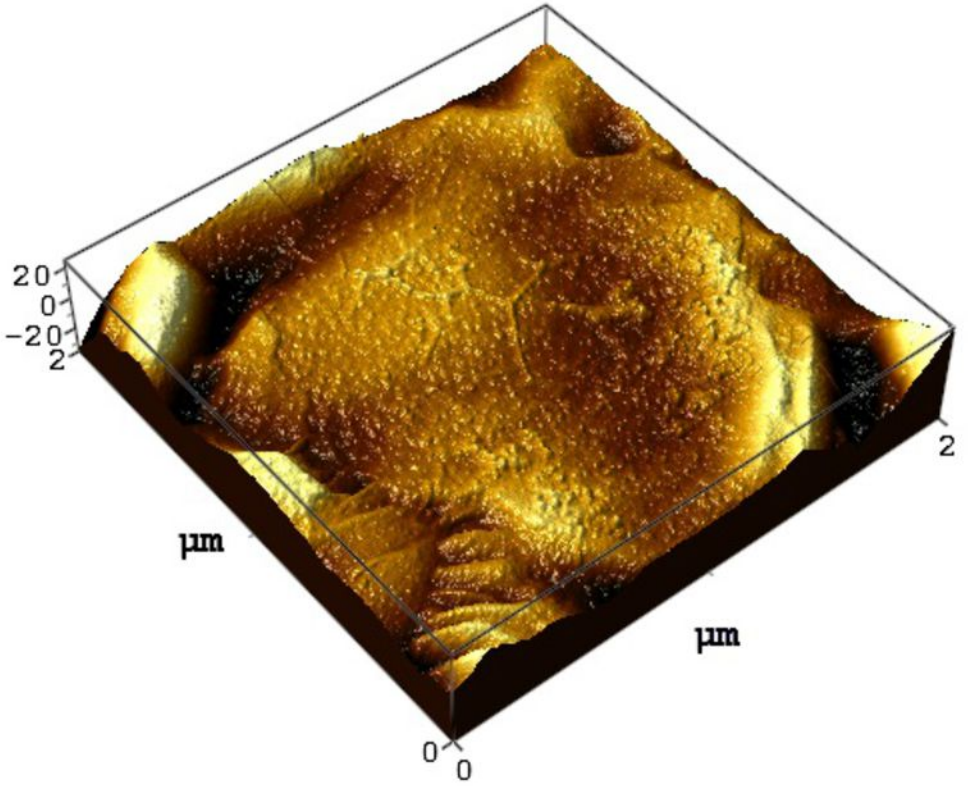
20
0
−20
2
µm
0
0
µm
2

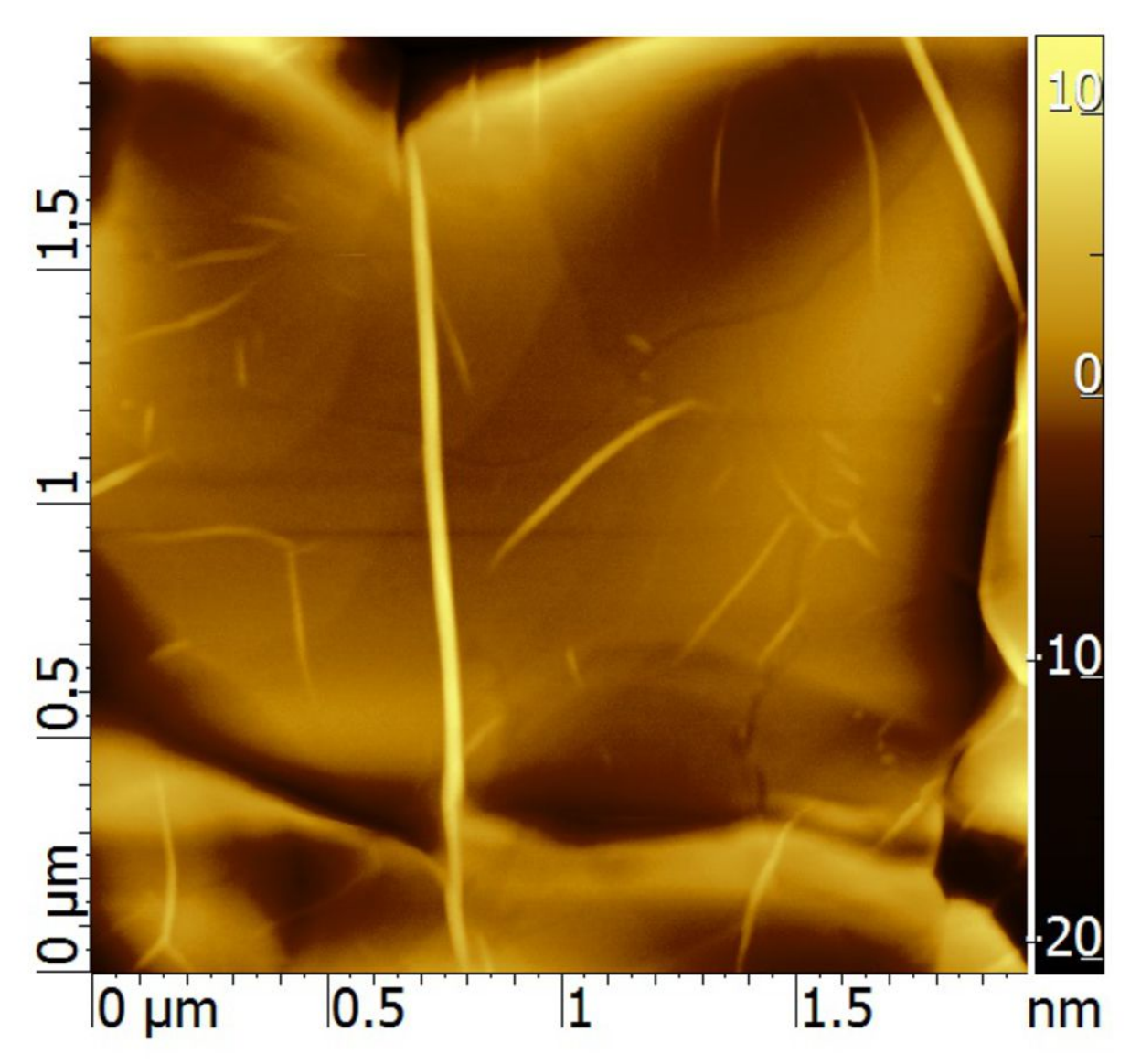
10
0
-10
-20
1.5
1
0.5
0 µm
0 µm
0.5
1
1.5
nm

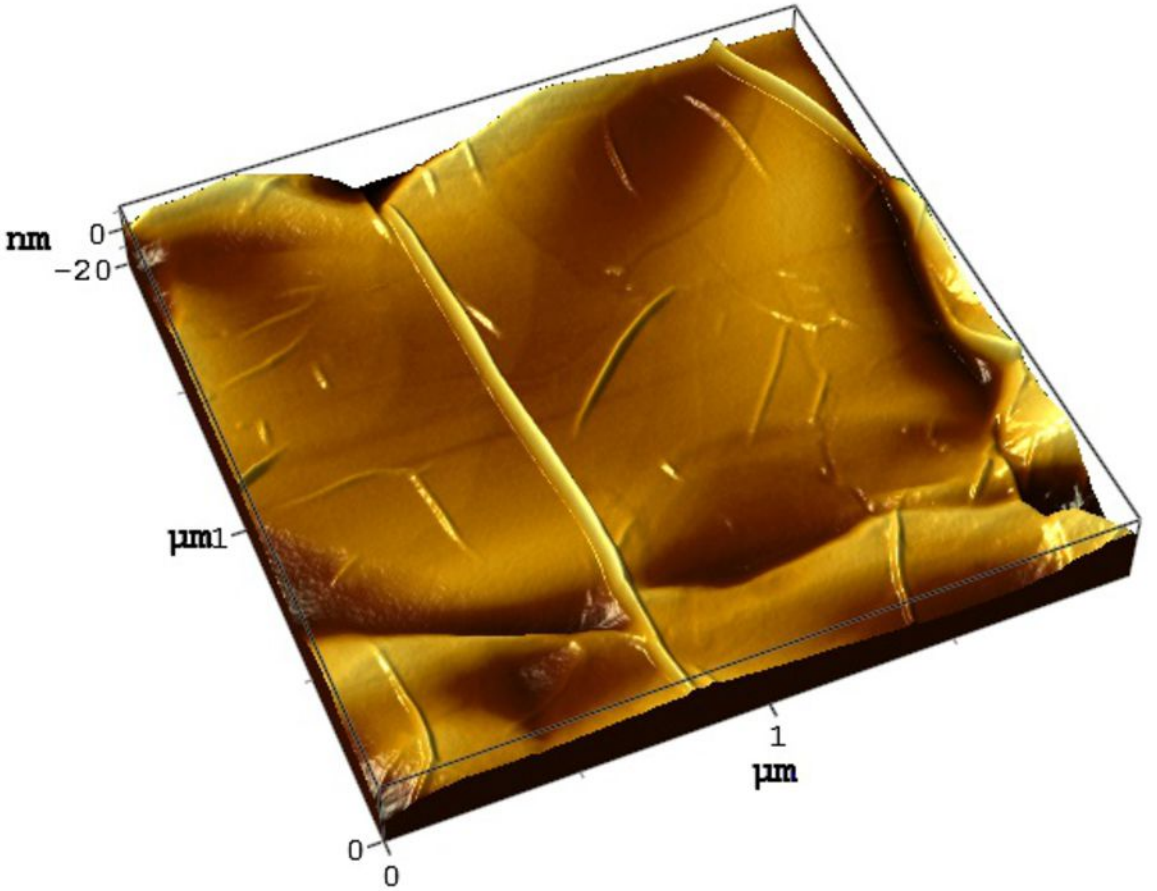
nm
0
−20
µm1
0
0
1
µm

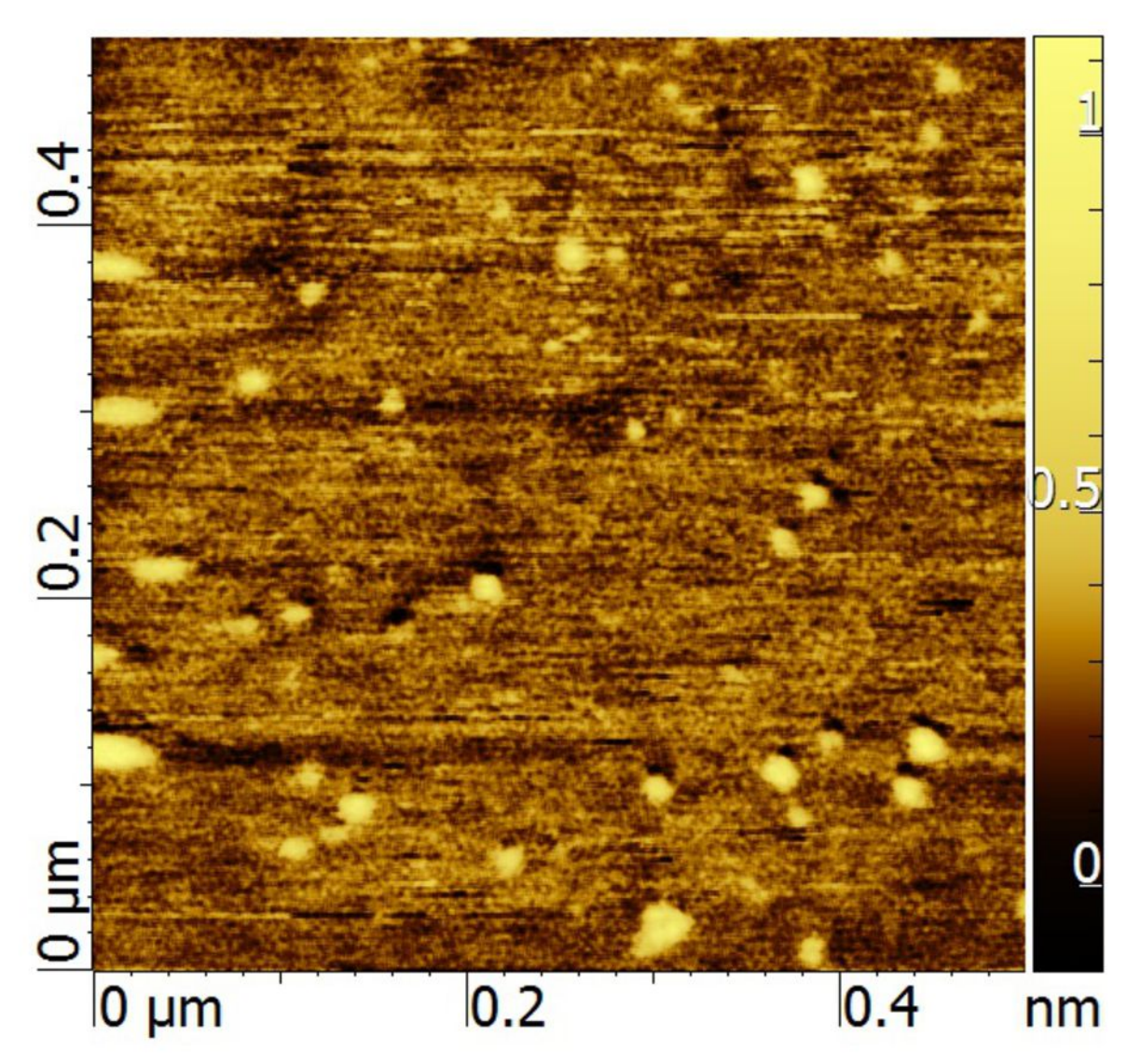
0.4
0.2
0 µm
0 µm
0.2
0.4
nm
1
0.5
0

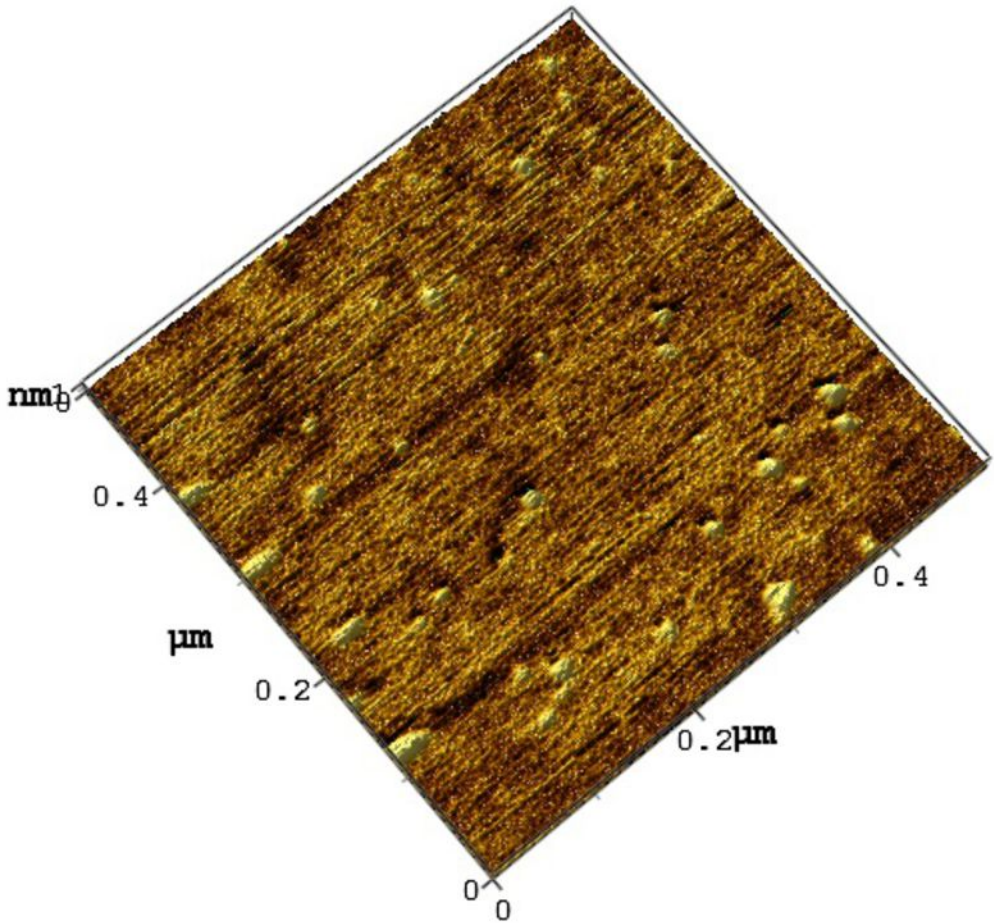
nm
0
0.4
µm
0.2
0
0
0.2µm
0.4

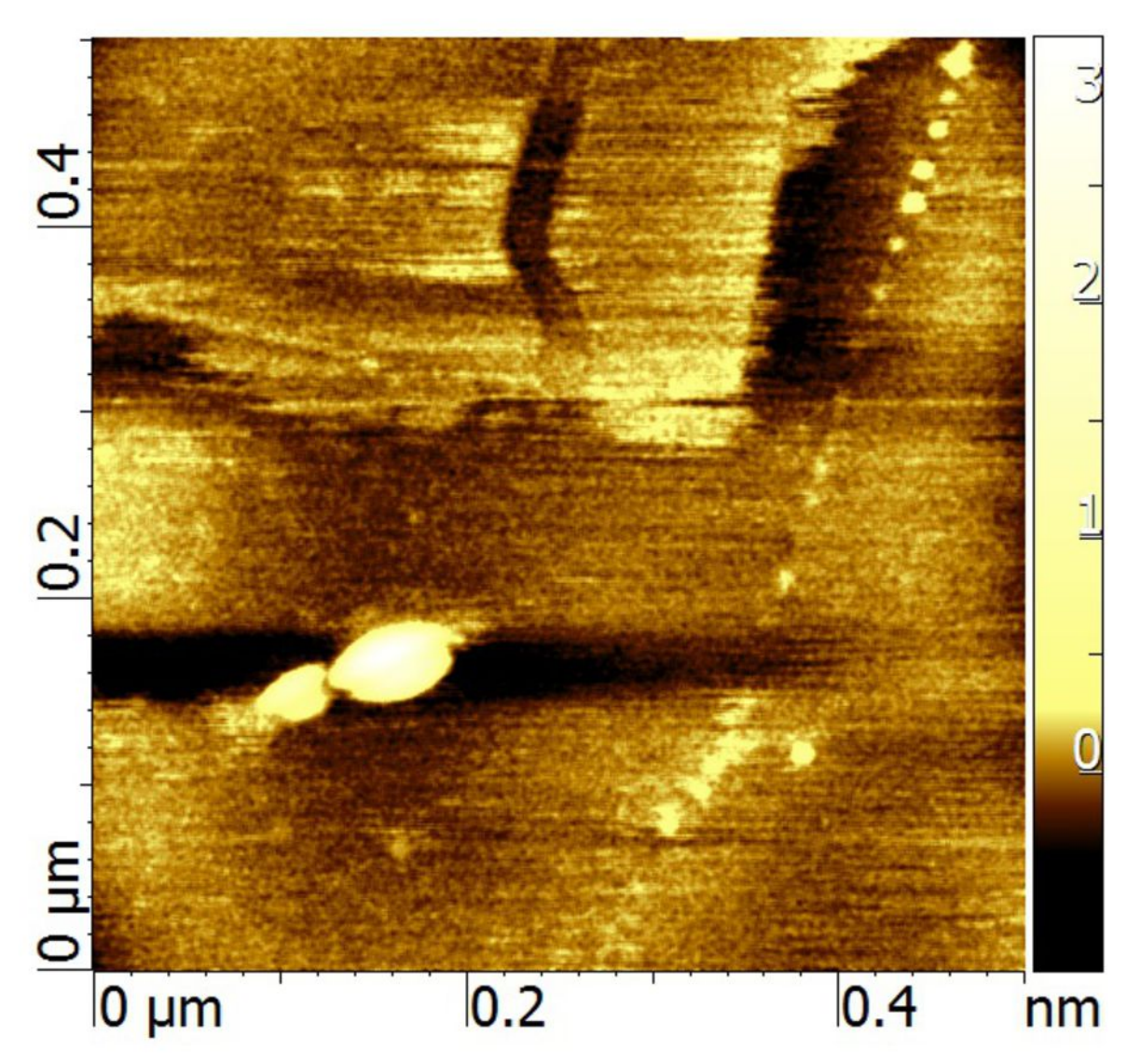
0.4
0.2
0 µm
0 µm
0.2
0.4
nm
3
2
1
0

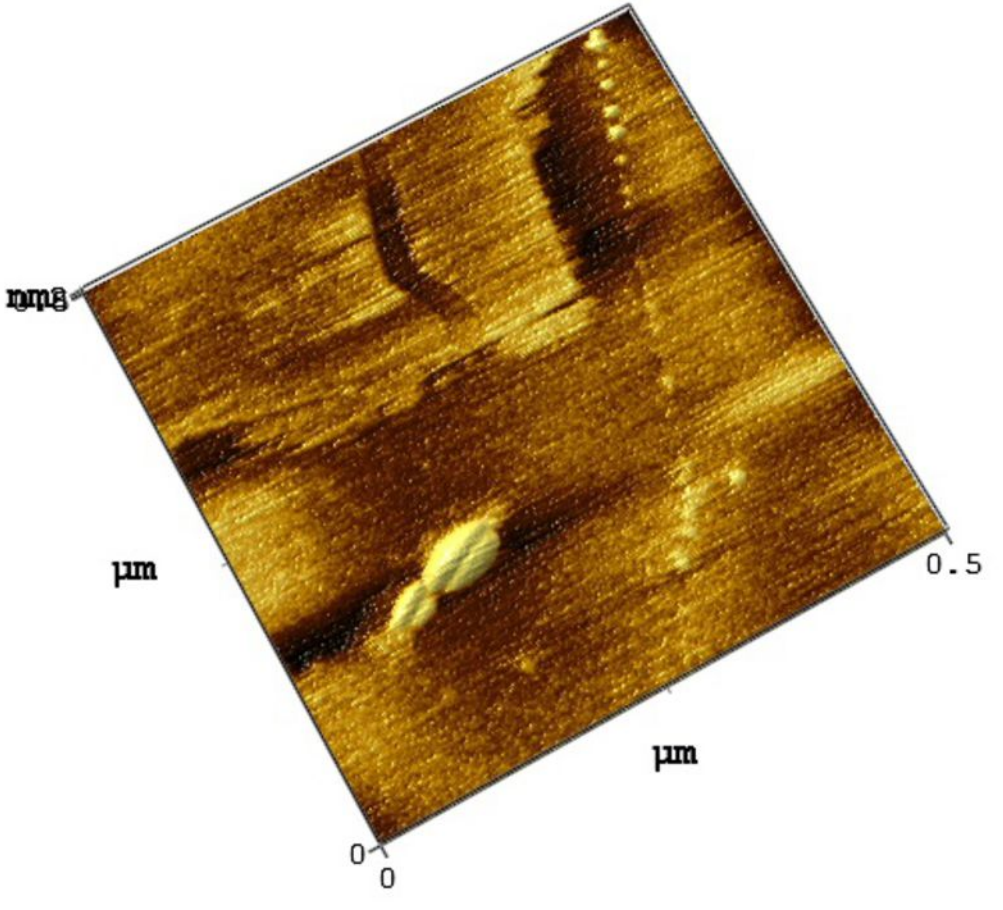
nm
µm
0.5
µm
0
0

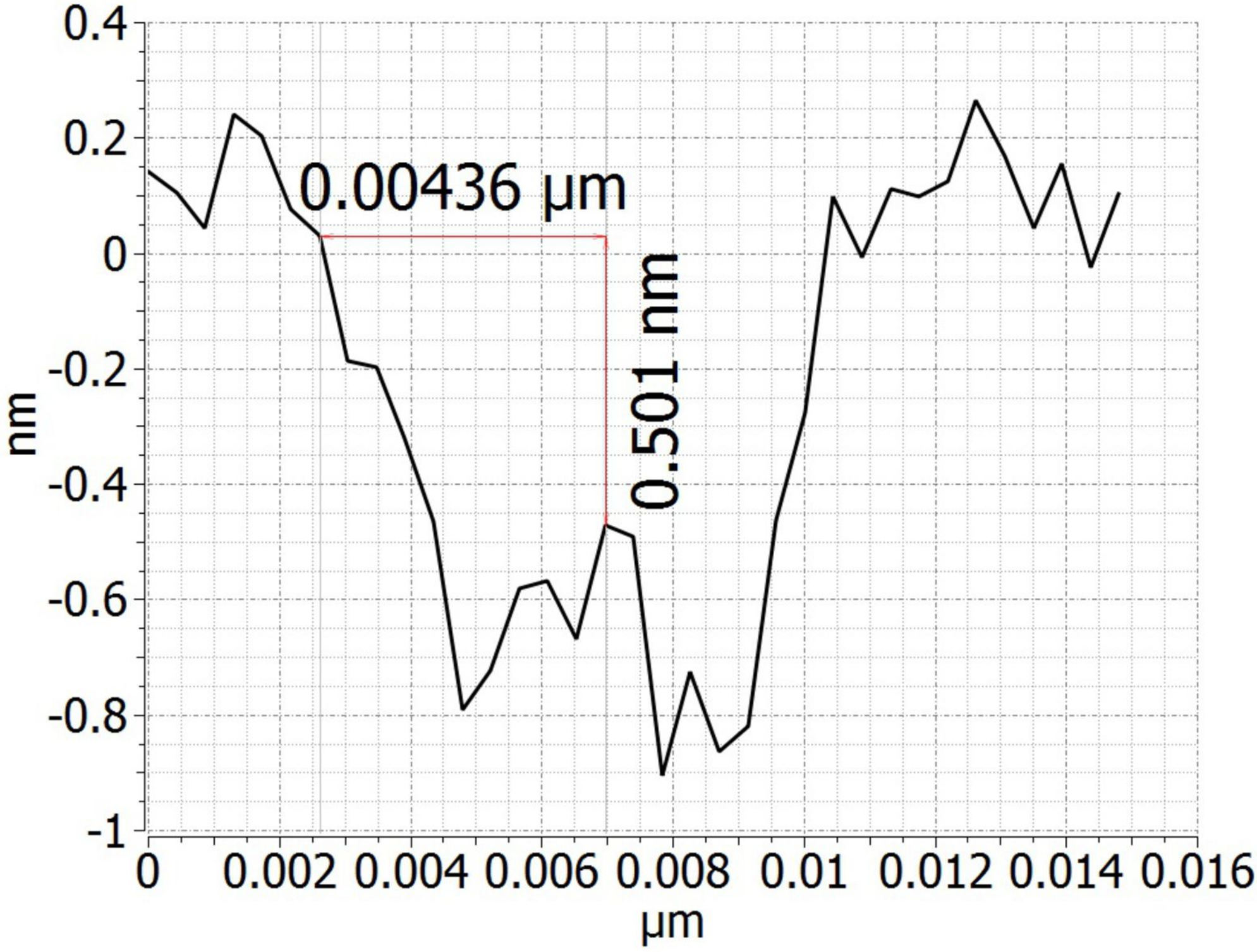
0.4
0.2
0
-0.2
-0.4
-0.6
-0.8
-1
nm
0.00436 µm
0.501 nm
0
0.002
0.004
0.006
0.008
0.01
0.012
0.014
0.016
µm

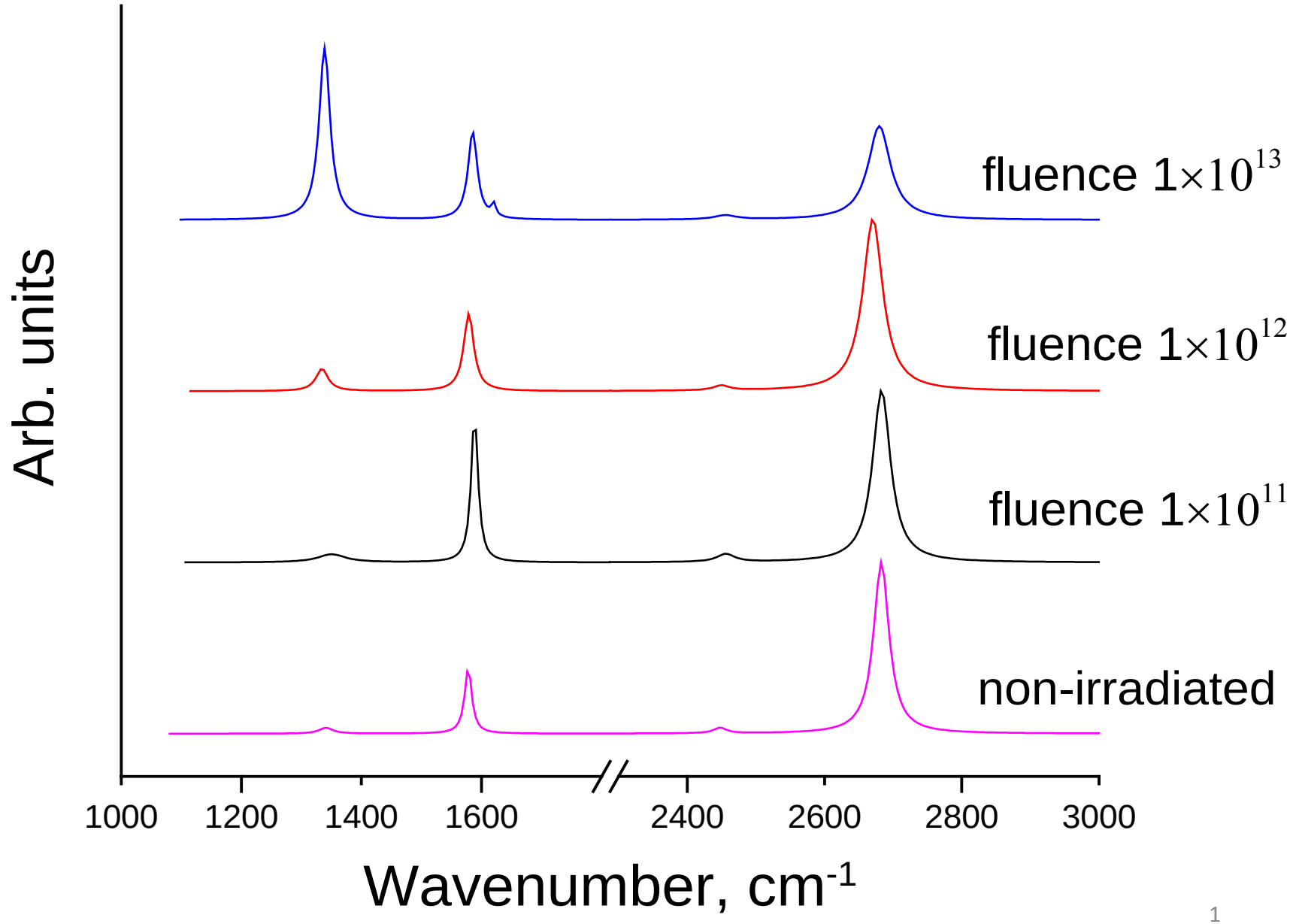
Arb. units
fluence 1×10^13
fluence 1×10^12
fluence 1×10^11
non-irradiated
1000
1200
1400
1600
2400
2600
2800
3000
Wavenumber, cm^-1

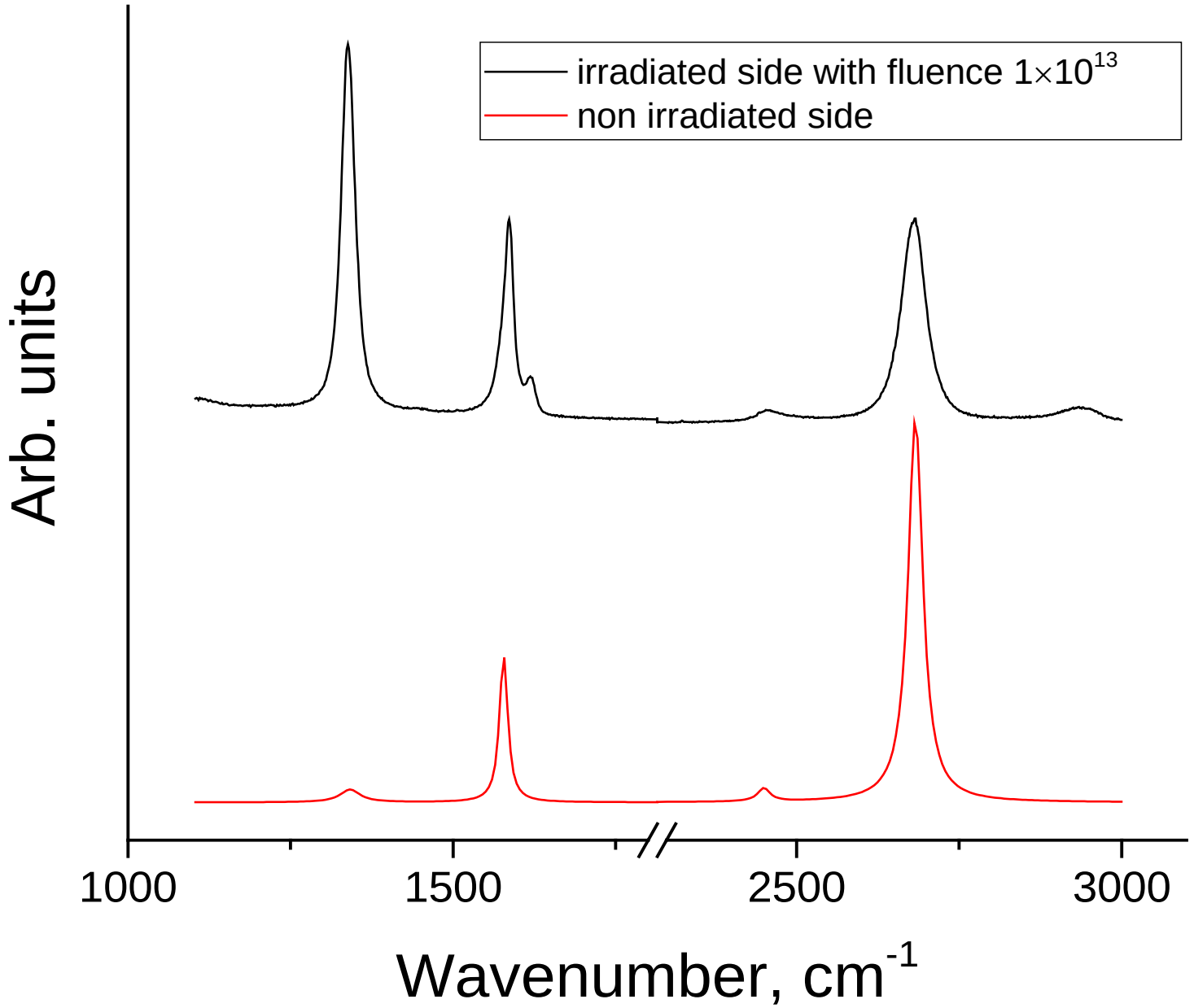
irradiated side with fluence 1×10^13
non irradiated side
Arb. units
1000
1500
2500
3000
Wavenumber, cm^-1

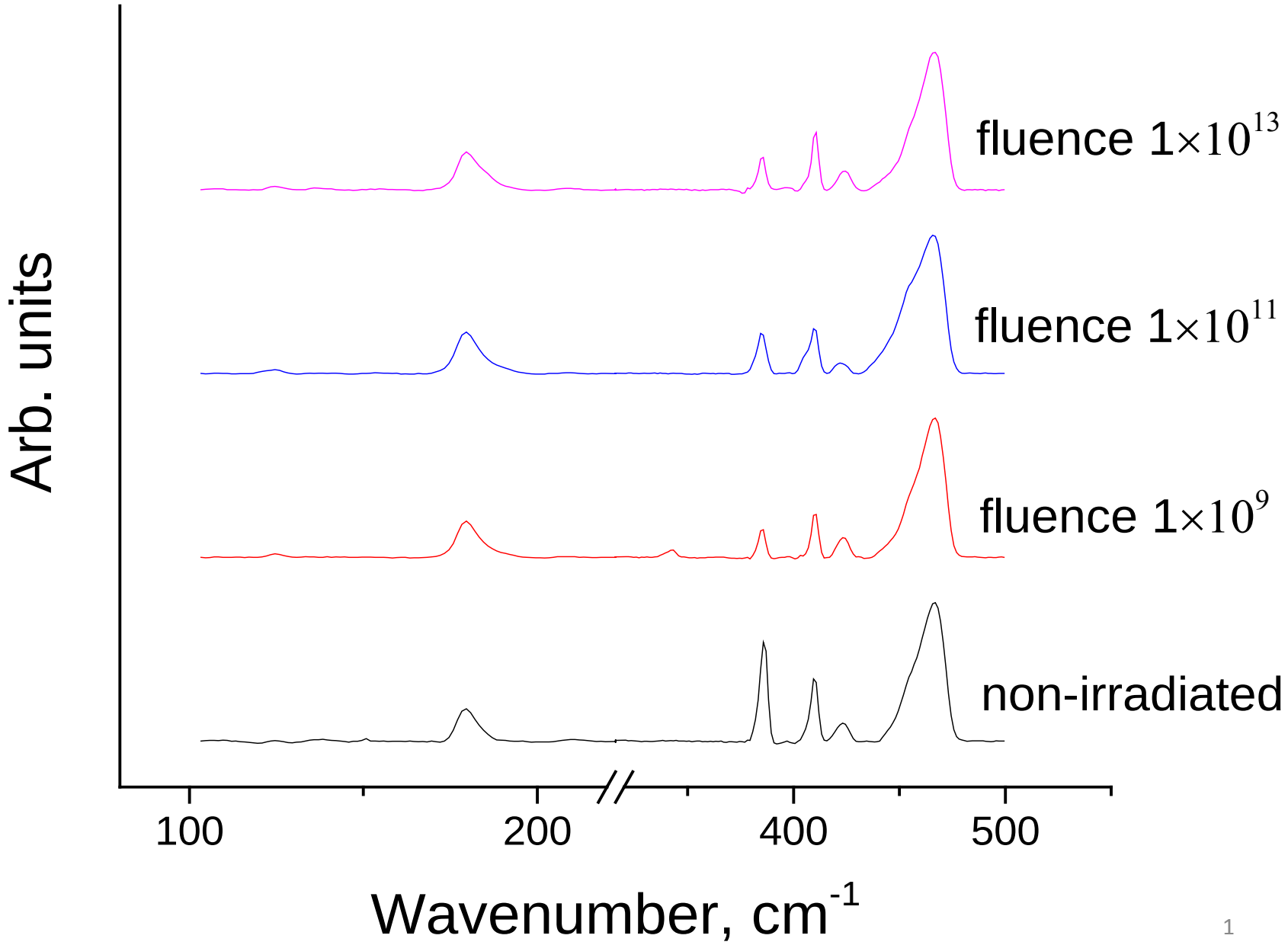
Arb. units
fluence 1×10^13
fluence 1×10^11
fluence 1×10^9
non-irradiated
100
200
400
500
Wavenumber, cm^-1